

# A Dynamical System for Plant Pattern Formation: A Rigorous Analysis

Pau Atela  
Dept. of Mathematics  
Smith College

Christophe Golé  
Dept. of Mathematics  
Smith College

Scott Hotton  
Dept. of Mathematics and Statistics  
Miami University

July 1, 2002

## Abstract

We present a rigorous mathematical analysis of a discrete dynamical system modeling plant pattern formation. In this model, based on the work of physicists Douady and Couder, fixed points are the spiral or helical lattices often occurring in plants. The frequent occurrence of the Fibonacci sequence in the number of visible spirals is explained by the stability of the fixed points in this system, as well as by the structure of their bifurcation diagram. We provide a detailed study of this diagram.

*Keywords: Phyllotaxis, pattern formation, Fibonacci, parastichy.*

## Contents

<b>1</b>	<b>Introduction</b>	<b>2</b>
1.1	Description of the Biological Phenomenon . . . . .	2
1.2	Preview of Results . . . . .	5
<b>2</b>	<b>A Dynamical System Model</b>	<b>7</b>
2.1	The Phase Space . . . . .	7
2.2	The Map $\Phi$ . . . . .	8
2.3	Least Crowded Spot: a Maximin Principle . . . . .	8
2.4	About the Choice of Dimension . . . . .	9
2.5	Making Use of Symmetry: the Map $\phi$ . . . . .	10
<b>3</b>	<b>Fixed Points for <math>\phi</math></b>	<b>10</b>
3.1	Fixed Points are Helical Lattices . . . . .	10
3.2	Stability of Fixed Points . . . . .	11

<b>4</b>	<b>Lattices</b>	<b>11</b>
4.1	Lattices and Parastichies . . . . .	11
4.2	Classification of Lattices . . . . .	13
4.2.1	The Fundamental Quadrilateral and Hexagon . . . . .	13
4.2.2	The Quadrilateral $Q_{mn}$ and the Hexagon $H_{mn}$ . . . . .	15
4.3	Branching Points of $\mathcal{V}$ . . . . .	17
<b>5</b>	<b>The Bifurcation Diagram</b>	<b>20</b>
5.1	Outline . . . . .	20
5.2	The Vertical Branch $\mathcal{L}$ of $\Sigma$ . . . . .	21
5.3	Opposed Rhombic Lattices . . . . .	22
5.3.1	Regular and Irregular Quadrilaterals . . . . .	22
5.3.2	Pruning the Tree, Fibonacci and Farey Rules . . . . .	23
5.4	Further Pruning: Requiring Global Maximum for $D$ . . . . .	24
5.5	Limits to Noble Numbers. End of Proof of Theorem 3 . . . . .	27
5.6	Monotonicity of Branches . . . . .	27
5.7	A Scenario for Fibonacci Phyllotaxis . . . . .	28
<b>6</b>	<b>Periodic Orbits</b>	<b>28</b>
<b>7</b>	<b>Comparison with Other Works</b>	<b>29</b>
<b>8</b>	<b>Appendix I: Proof of Theorem 2</b>	<b>32</b>
<b>9</b>	<b>Appendix II: Proof of Proposition 5.5</b>	<b>33</b>

# 1 Introduction

## 1.1 Description of the Biological Phenomenon

There are hundreds of thousands of species of plants exhibiting a huge diversity of plant forms. Yet despite this diversity there are only a few ways in which botanical units such as leaves, florets or scales are arranged along a stem. The study of these plant patterns is known as *phyllotaxis*.

It is conventional to classify phyllotactic patterns into three broad categories: whorled, spiral and distichous. Whorled phyllotaxis is characterized by two or more botanical units growing from the same region, or *node*, of a stem. In spiral phyllotaxis only one botanical unit grows at each node and the angle between successive units, called the *divergence angle*, is constant. Distichous phyllotaxis can be seen as a special case of spiral phyllotaxis where the divergence angle is  $180^\circ$ . While in distichous phyllotaxis there are two rows along the stem, in spiral phyllotaxis there are two main visible families of spirals or helices called *parastichies* (see Figures 1 and 2).

One of the more remarkable features of spiral phyllotaxis is that the number of spirals or helices in the two families tend to be two consecutive elements in the Fibonacci sequence  $1, 1, 2, 3, 5, 8, 13, 21, 34, \dots$  ( $F_{n+1} = F_n + F_{n-1}$ ) (see



Figure 1: The pine cone shown on the left displays 13 spirals winding as the one shown in black, and 8 winding as the one shown in white. These spirals, joining scales to their nearest neighbors, are called parastichies. The pineapple shows a similar structure, but its parastichies are helices. On the right, one of the mathematical models (a helical lattice) studied in this paper.

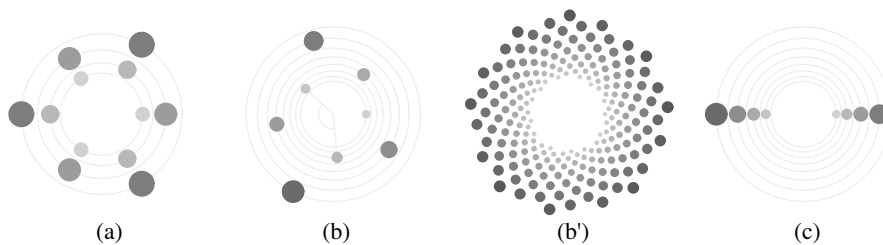


Figure 2: The three main phyllotactic types in a disk (or centric) representation: (a) whorled (here 3 botanical units appear at each node); (b) spiral, with divergence angle  $\simeq 137.5^\circ$ ; (b') spiral again, with same divergence angle but lower growth rate; (c) distichous.

Figure 1). Moreover, the divergence angle between two successive elements tends to  $360^\circ(\tau) \simeq 222.492^\circ$  (or  $360^\circ(1 - \tau) \simeq 137.507^\circ$ ) where  $\tau$  is the golden ratio  $\tau = \frac{-1+\sqrt{5}}{2} = 0.61803\dots$  (see Figure 2). This is the most well known phenomenon studied in the interdisciplinary field of Phyllotaxis.

Phyllotactic patterns are established at a microscopic scale by a process known as *meristematic development*. For example, the patterns seen in large sunflower heads are actually established when the sunflower's blossom is only  $2\text{ mm}$  in diameter. The botanical units or plant organs composing these patterns are formed in the small shoot apices of plants. They first appear at the usually circular edge of an apex (or *apical meristem*) as bulges of cells called *primordia* (see Figure 3). The biological mechanism of primordium formation is still unknown, although various hypotheses have been brought forward such as anisotropic concentrations of morphogens [30] or inhibitory chemical substances [23] (yet to be determined), or buckling of a layer of cells (tunica) over the core (corpus) of the apex [11].



Figure 3: On the left, two scanning electron microscope pictures of a magnolia apex (size  $\simeq 2\text{ mm}$ ). On the right, a stylized view of a plant apex. New primordia form as far away as possible from existing primordia. Once formed, primordia move radially away from the center of the apex.

Phyllotactic patterns are not fixed characteristics of a plant species. Examples of whorled, distichous, and spiral phyllotaxis can be found in almost every plant family. Furthermore, it is very common for leaves on a plant to exhibit distichous phyllotaxis during the early stages of growth and to undergo a transformation to spiral phyllotaxis shortly before the plant flowers. Typically, in such plants the floral organs continue to display spiral phyllotaxis. On the other hand, in some other plants (such as Bromeliads) the leaves display spiral phyllotaxis in the early stages of growth and undergo a transformation to distichous phyllotaxis which continues on with the floral organs.

Each type of phyllotactic pattern results from a particular developmental sequence. The fact that the different types of phyllotaxis occur in almost every plant family while an individual plant can exhibit different types of phyllotaxis at different stages indicates that the process of meristematic development is very similar among the higher plants. The different types of phyllotaxis can result from a single process operating under different initial conditions and parameter values. The transformation from one phyllotactic pattern to another in an individual plant can be a consequence of a parameter varying as the plant grows.

In 1868 the botanist Hofmeister [13] published his results on the microscopic study of plant shoot apices. Based on his observations he proposed that when a single primordium forms, it always does so in the least crowded spot along the apical ring. This is seen as a consequence of primordia exerting an inhibitory effect on the formation of new primordia, whether it be chemical or bio-mechanical. Following Douady and Couder [7], we add a few simple rules to this:

### Hofmeister Hypotheses

- (i) The apex has an axis of symmetry.
- (ii) Primordia form at the edge of the apex and, due to the shoot's growth, they move away radially from the center with radial velocity only depending on their distance to the edge of the apex.
- (iii) New primordia are formed periodically, the period is called the *plastochrone*.

- (iv) The incipient primordium forms in the largest available space left by the previous ones.

The region of the apex where primordia form can be approximated by many different shapes: a flat annulus, a section of a cone, of a cylinder or of a paraboloid, and others. Numerical experiments we and others have performed show that there are no drastic qualitative differences in the phenomena observed when we change shapes. We choose here a cylindrical shape, since the analysis is much simpler than in the other cases, and assume a constant velocity of transport for the primordia.

## 1.2 Preview of Results

In this paper, we address two simple and yet fundamental questions:

- (1) Why do spiral or helical lattices occur so predominantly?
- (2) Why, among these lattices, do the ones exhibiting Fibonacci parastichy numbers occur most often?

Many models assume that there is a lattice structure and address only the second question (*e.g.*, [1, 18]). Numerical simulations have also been performed, most notably by Douady and Couder [7]. This paper studies a parameterized family of discrete dynamical systems that models meristematic development and which gives answers to both questions. It should be noted that while Douady and Couder as well as many others have used the terminology of dynamical systems, aside from Kunz [16] this conceptual step has not been performed before. Moreover, because of its relative simplicity, our model allows complete and rigorous *mathematical* answers to these questions. Our model is a one-parameter family of discrete dynamical systems on a high dimensional torus. It is based on phenomenological observations by the botanist Hofmeister [13] (see above), as revisited by Douady and Couder [7]. This model also shows how, as the parameter is varied, a transition occurs between distichous and spiral phyllotaxis.

Theorem 1 shows that all fixed points of our system are lattice configurations. In Theorem 2, we prove that all fixed points are stable, accounting for their widespread occurrence in nature. The parameter we use for a cylindrical shaped apex is the *internodal* distance, *i.e.*, the distance between neighboring nodes. Theorem 3 describes the structure of the bifurcation diagram of our system as the parameter (internodal distance) varies: it is a “pruned” van Iterson diagram (see Figure 4).

When the internodal distance is large, there is only one branch in the diagram. On this branch the divergence angle is  $180^\circ$ , corresponding to distichous phyllotaxis. As the internodal distance decreases, we reach the point  $A^*$ . Here we have an unusual type of symmetry breaking bifurcation (Section 5.7). As the parameter decreases, the distichous branch ceases to exist and two new branches descend from  $A^*$ . These two branches correspond to lattices of opposite chirality. As the parameter is decreased further, these branches tend in the limit to

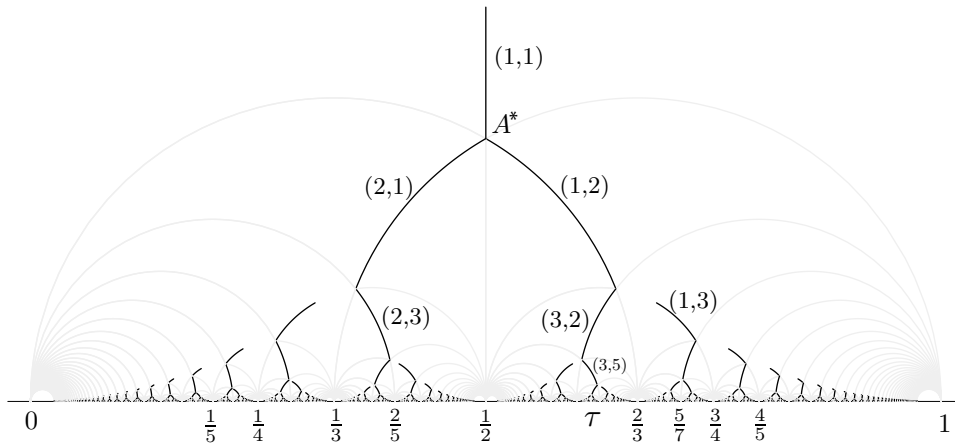


Figure 4: The fixed point bifurcation diagram (in black) and its underlying hyperbolic geometry (in grey). Each point of the bifurcation diagram corresponds to a fixed point of the system, a helical lattice with constant divergence angle. The horizontal axis is the divergence angle measured as a fraction of a turn. The vertical axis is the parameter in the system, the internodal distance. The parastichy numbers of the fixed points vary from segment to segment in the bifurcation diagram, in the figure some of these are labeled  $(i, j)$ . The parastichy numbers of distichous phyllotaxis are  $(1, 1)$ . The point  $A^*$  is a symmetry breaking bifurcation point, where a transition from distichous to spiral phyllotaxis occurs.

the numbers  $1 - \tau$  and  $\tau$  on the horizontal axis. Moreover, as we follow these two branches, the parastichy numbers of the lattices follow the Fibonacci sequence.

The stability of the fixed points and the structure of the bifurcation diagram can be used to answer the second question. In the early stages of a plant's growth the internodal distance is large and the plant exhibits distichous phyllotaxis. As the plant grows, the internodal distance decreases, the phyllotaxis is transformed to spiral type, and the parastichy numbers of the plant become consecutive Fibonacci numbers. This decrease in internodal distance is supported by botanical evidence [20, 25, 33]. In terms of our dynamical system, if a configuration is near a fixed point and we decrease the parameter (internodal distance) while iterating the map, the successive configurations will follow closely a branch of the bifurcation diagram.

What is also interesting is the fact that there are other branches in the bifurcation diagram. The lattices on the largest pair of these other branches follow the Lucas sequence  $(1, 3, 4, 7, 11, \dots)$ . Although Lucas numbers are much less common in spiral phyllotaxis, they do occur. Furthermore, plants have been observed to display pairs of smaller Lucas numbers in the early stages of growth and pairs of larger Lucas numbers in their later stages.

Since the complete biological mechanisms of primordium formation are yet unknown, we do not claim an exhaustive rendition of all the parameters and

phenomena at play (other models and their relationship with this one are discussed in Section 7). Instead, we hope that our model points to some universal (hence, simplest in some sense) mathematical features that we think should be present in all models of phyllotaxis. Moreover, despite its simplicity, this model yields patterns (periodic orbits) that do occur in plants but are very seldom mentioned by botanists (see Section 6). We hope that a classification of such patterns will yield a better understanding of the transitions between whorl and spiral patterns.

This paper bears a lot in common with Kunz’s thesis [16] who independently discovered a dynamical system, similar to ours, which fits Douady and Couder’s model. In contrast to Kunz’s system, ours only takes into account the influence of the closest primordium on the nascent one. This greatly simplifies the analysis of the bifurcation diagram and allows complete mathematical rigor. The (structural) stability of the fixed points in our system and the lack of agreement among biologists as to the precise nature of the mutual “inhibition” between primordia further legitimize the simplicity of our assumption. Adler [1] makes a similar assumption in a (non-dynamical) lattice model. Levitov [18] introduces, in the context of lattices of superconductivity, a model similar to Adler’s and uses hyperbolic geometry techniques which influenced this work. Finally, Douady [6] obtains the same bifurcation diagram as ours using a disk packing interpretation of the phenomenon. In Section 7 we review in more detail the relation of these and other authors’ works to ours.

The web site [www.math.smith.edu/~phyll](http://www.math.smith.edu/~phyll) contains interactive applets illustrating some of the concepts studied in this paper.

## 2 A Dynamical System Model

We remind the reader that a discrete dynamical system is simply a map  $\phi : E \rightarrow E$  where  $E$ , called the phase space, is usually a topological space. One is interested in *orbits* of  $\phi$ , defined by  $x_n = \phi(x_{n-1})$ . We will define two related discrete dynamical systems based on the above Hofmeister hypotheses.

### 2.1 The Phase Space

For simplicity of the analysis, we work in the cylindrical representation of Phyllotaxis, which we can think of, for example, as leaf primordia forming along a stem. We represent the stem of our plant upside down, as the half cylinder  $\mathcal{C} = \mathbb{S}^1 \times [0, \infty)$  with unit circumference. The edge of the apical meristem, where new primordia are born, is the circle  $\mathbb{S}^1 \times \{0\}$  (see Figure 5). Primordia are idealized as points in  $\mathcal{C}$  and indexed backwards:  $p_k$  denotes the primordium that appeared  $k$  plastochrones ago (recall that a plastochrone is the elapsed time between two consecutively formed primordia),  $p_0$  is the most recently formed primordium, located at the edge of  $\mathcal{C}$ . A possible configuration can be described as  $\{p_0, p_1 \dots, p_N\}$ , where  $p_k = (\theta_k, y_k)$  has angular and vertical coordinates. The periodicity condition in the Hofmeister hypotheses implies that the pri-

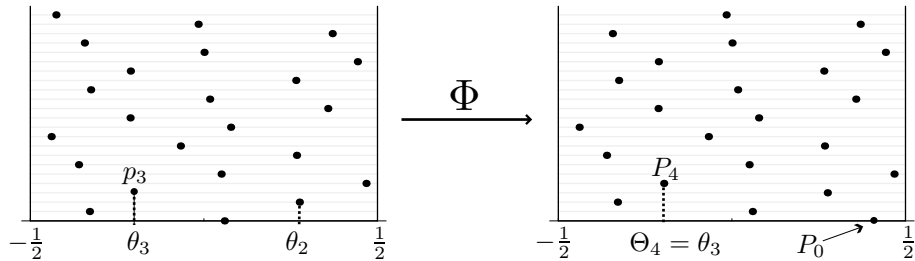


Figure 5: A configuration on the unrolled half cylinder and its image under one iteration of the map  $\Phi$ .

primordia have a constant vertical interspacing. This simply translates to  $y_k = ky$  for a fixed parameter  $y > 0$  called the *intermodal distance*. Once the parameter  $y$  is fixed, configurations are determined uniquely by their angular coordinates  $\theta_k$ . Hence, the phase space our map  $\Phi$  (defined below) acts on is the  $N + 1$ -torus  $\mathbb{T}^{N+1}$ , with coordinates  $(\theta_0, \theta_1, \dots, \theta_N)$ . Figure 5 shows a configuration with an illustration of the notation just introduced.

## 2.2 The Map $\Phi$

Given a configuration  $\{p_0, \dots, p_N\}$  of primordia, we denote by  $\{P_0, P_1, \dots, P_N\}$  the new configuration of primordia after one plastochrone. We now define what the “new”  $P_k$  are. According to Hofmeister hypotheses, primordium  $p_k = (\theta_k, y_k) = (\theta_k, ky)$  has moved up by  $y$ , becoming primordium  $P_{k+1}$ . Therefore, we define  $P_{k+1} = (\Theta_{k+1}, Y_{k+1}) = (\theta_k, (k+1)y)$ . The incipient primordium  $P_0 = (\Theta_0, 0)$  appears in the “least crowded spot” left by the other  $P_k$ ’s. This defines a map  $\Phi : \mathbb{T}^{N+1} \rightarrow \mathbb{T}^{N+1}$  of the following form:

$$\begin{aligned} \Theta_0 &= F(\theta_0, \dots, \theta_N) \\ \Theta_1 &= \theta_0 \\ &\vdots \\ \Theta_N &= \theta_{N-1} \end{aligned}$$

where  $F$ , whose precise definition is given in the next subsection, is a function implementing Hofmeister’s condition of “least crowded spot”.

## 2.3 Least Crowded Spot: a Maximin Principle

We now turn to the definition of  $F$ . The “crowdedness” will be measured by some “inhibitory field”. We choose to measure the amount of inhibition felt at

a location  $p$  on the circle  $\mathbb{S}^1 \times \{0\}$  by the distance between  $p$  and the closest primordium:

$$D(p) \stackrel{\text{def}}{=} \min_{1, \dots, N} \|P_k - p\|.$$

The smaller this minimum distance  $D(p)$  is, the more inhibition is felt at  $p$ . The location for the new primordium  $P_0 = (\Theta_0, 0)$  should thus be where the least inhibition is felt, *i.e.*, we want to maximize  $D$ . Therefore, we define  $P_0$  as the location such that

$$D(P_0) = \max_{p \in \mathbb{S}^1 \times \{0\}} D(p).$$

This defines  $\Theta_0 = F(\theta_0, \dots, \theta_N)$ , and we refer to it as the *Maximin Principle*. We note that occasionally there is more than one location where this maximum is achieved, we study this in Section 5.4. The Maximin Principle has two geometric consequences that will be crucial in the characterization of fixed points (Section 5): the incipient primordium  $P_0$  must be *equidistant* from its two nearest neighbors, say  $P_n$  and  $P_m$ ; furthermore,  $P_n$  and  $P_m$  must lay on *opposite sides* of  $P_0$ . These statements only make sense when we unroll the cylinder on the plane, *i.e.*, when we consider its covering space. The caption of Figure 6 gives a trivial “proof” of these two facts.

**Remark.** We chose the above definition of “least crowdedness” because it is the simplest that yields the full phenomenon. Moreover, it allows a complete and rigorous mathematical analysis and the stability results of Theorem 2 ensure that any nearby model will exhibit the same phenomenon (structural stability). See Section 7 for comparison with other definitions of “least crowdedness”.

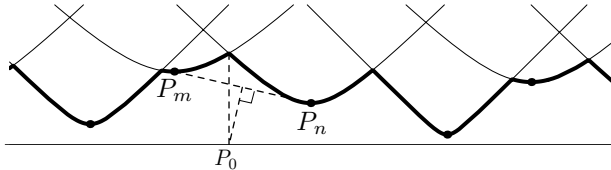


Figure 6: The minimum distance function  $D$  is the lower envelope of the graphs of the functions  $D_k(p) = \|P_k - p\|$ . Since each  $D_k$  is convex, a maximum of  $D$  must occur where the graphs of  $D_n$  and  $D_m$  meet, for some  $n$  and  $m$ . Such a point  $P_0$  must be equidistant from  $P_n$  and  $P_m$ , hence it lies on their perpendicular bisector. Moreover, for  $D$  to increase to the left of  $P_0$  and decrease to the right, the point  $P_0$  must be to the right of one of  $P_n$  or  $P_m$  and to the left of the other.

## 2.4 About the Choice of Dimension

The fixed number  $N$  should be large enough so that  $P_N$  does not have any effect on  $D$  regardless of the position of all the other primordia. The worst case scenario is a configuration with  $P_k$ ,  $0 < k < N$ , aligned at positions  $(\frac{1}{2}, ky)$ . One can check that  $N > \frac{1}{2y} + 1$  is enough.

Requiring a fixed number of primordia seems artificial in terms of botany, where the number of primordia is always increasing. But note that configurations of  $N'$  primordia, with  $N' < N$  are in fact included in our space of configurations  $\mathbb{T}^{N+1}$ : such a configuration  $\{p_0, p_1, \dots, p_{N'}\}$  is completely equivalent (dynamically) to one in which we add “virtual” primordia  $p_{N'+1}, \dots, p_N$  all placed exactly “behind”  $p_{N'}$ . That is with  $\theta_{N'} = \theta_{N'+1} = \dots = \theta_N$ .

## 2.5 Making Use of Symmetry: the Map $\phi$

Our system has rotational symmetry: we are interested in the shape of a configuration, not its location around the stem. The configuration shapes are thus determined up to a rotation around the circle. The easiest way to account for this symmetry is to introduce relative angle coordinates  $x_k = \theta_{k+1} - \theta_k$ , called *divergence angles* by botanists. This gives rise to another map  $\phi$  on the  $N$ -torus  $\mathbb{T}^N$  parametrized by the divergence angles  $(x_0, \dots, x_{N-1})$ . To define  $\phi$  rigorously, consider the map

$$S : (\theta_0, \dots, \theta_N) \rightarrow (\theta_1 - \theta_0, \dots, \theta_N - \theta_{N-1}) = (x_0, \dots, x_{N-1})$$

between absolute angle and divergence angle coordinates. Then  $\phi$  is uniquely defined by the relation

$$S \circ \Phi = \phi \circ S.$$

## 3 Fixed Points for $\phi$

A configuration with a constant divergence angle is a helical lattice. As noted in the introduction, helical lattices are configurations that very often occur in nature. An essential feature of our model is that the kinds of helical lattices observed in plants appear as fixed points of the map  $\phi$  defined above (Section 5 shows exactly which helical lattices appear as fixed points of the dynamical system). Furthermore, these fixed points are stable: the iterates of all configurations in a neighborhood of a fixed point converge to it, accounting for the robustness of the phenomenon and its occurrence in nature.

In this section, we show that fixed points are helical lattices and state the stability theorem of fixed points. Its proof appears in Appendix I.

### 3.1 Fixed Points are Helical Lattices

**Theorem 1.** *Fixed points of  $\phi$  are helical lattices, i.e., configurations with constant divergence angles.*

*Proof.* Let  $(X_0, \dots, X_{N-1}) = \phi(x_0, \dots, x_{N-1})$ . A fixed point is such that  $X_k = x_k$ ,  $k \in \{0, \dots, N-1\}$ . On the other hand, the definition of the map gives  $X_k = x_{k-1}$ ,  $k \in \{1, \dots, N-1\}$ . Hence,  $x_k = x_{k-1}$ ,  $k \in \{1, \dots, N-1\}$ : the divergence angle is constant.  $\square$

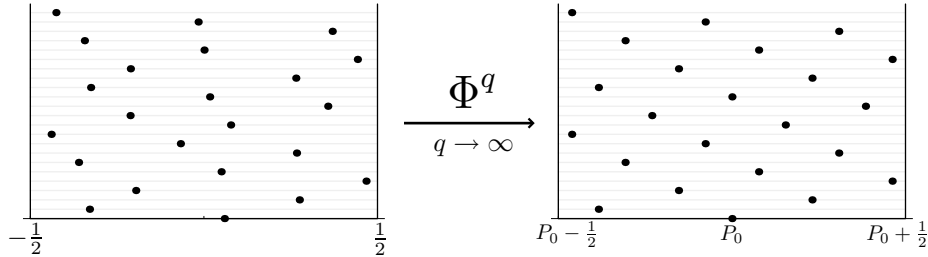


Figure 7: The limiting image of a configuration after repeated iterations of  $\Phi$ . In this case, the limit is a fixed point of the map  $\phi$ , a helical lattice.

### 3.2 Stability of Fixed Points

**Theorem 2.** *All fixed points are asymptotically stable: the spectrum of the differential of  $\phi$  is contained in the open unit disk.*

The proof, which uses some results of the subsequent sections, is in Appendix I. Figure 7 shows the convergence of a configuration to a helical lattice under iteration of the map  $\Phi$ .

## 4 Lattices

### 4.1 Lattices and Parastichies

In order to characterize those helical lattices that correspond to fixed points of the dynamical system, we need to define certain geometrical features of helical lattices and their parastichies.

A helical lattice is a discrete subgroup of the cylinder (isomorphic to  $\mathbb{Z}$ ) generated by a single fixed element  $(x, y)$  where, in the language of botany,  $x$  is the constant divergence angle and  $y$  is the internodal spacing. We use the notation  $L(x, y)$  to denote the helical lattice generated by  $(x, y)$ . Elements of  $L(x, y)$  are of the form  $(kx, ky)$ ,  $k \in \mathbb{Z}$  (the first coordinate is understood to be in  $\mathbb{R}/\mathbb{Z}$ ). Botanists (see, for example, [10]) have found it convenient to study helical lattices by looking at their covering spaces, which are planar lattices. This is conceived of as “unrolling” the cylinder  $\mathcal{C}$ . Since  $\mathcal{C}$  has circumference 1, when we lift or “unroll” the helical lattice generated by  $(x, y)$  we get the *planar lattice*  $\Lambda(x, y)$  generated by  $(x, y)$  and  $(1, 0)$  (where it is understood that  $x \in [0, 1)$ ). Hence,

$$\Lambda(x, y) = \{k(x, y) + d(1, 0) \mid k, d \in \mathbb{Z}\}.$$

We also use the complex notation  $z = x + iy$  and  $\Lambda(z)$  for  $\Lambda(x, y)$ . With this notation, points in  $\Lambda(z)$  are of the form  $kz + d$ , with  $k, d \in \mathbb{Z}$ .

Conversely, we conceive of the projection of a planar lattice to a helical lattice as a “rolling up” of the planar lattice. It is sufficient to project just the lattice points in the infinite strip  $(-\frac{1}{2}, \frac{1}{2}) \times \mathbb{R}$  (or  $\{w \in \mathbb{C} \mid \text{Re}(w) \in (-1/2, 1/2]\}$ )

to recover all of  $L(x, y)$  (this choice of strip picks up the representative of each element of  $L(x, y)$  which is closest to the origin). So we can imagine that the projection works by cutting the strip from the plane and gluing its edges together. Given a point  $(kx, ky) + (d, 0)$  in  $\Lambda(x, y)$ , its representative in the strip is  $(kx - \Delta_k(x), ky)$  where  $\Delta_k(x)$  is the closest integer to  $kx$ . (If there are two such integers, pick the smallest one.)

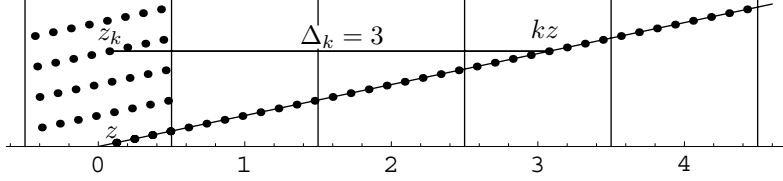


Figure 8: Geometric meaning of the encyclic number  $\Delta_k$ .

Botanists abbreviate  $\Delta_k(x)$  to  $\Delta_k$  and call it the  $k^{\text{th}}$  *encyclic number*. They also use the notation  $\delta_k = kx - \Delta_k$  which they call the  $k^{\text{th}}$  *secondary divergence angle*. Hence, the helical lattice  $L(x, y)$  has a one-to-one planar representation in the strip  $-1/2 < x \leq 1/2$  as  $\{(\delta_k, ky) \mid k \in \mathbb{Z}\}$ . We also use the complex notation for these favored representatives:

$$z_k = \delta_k +iky = kx - \Delta_k +iky = kz - \Delta_k.$$

When we lift a helix passing through the points of a helical lattice, we get a line that passes through the points of the corresponding planar lattice. We take the point  $p_k = (\delta_k, ky)$  of a helical lattice, lift it to the corresponding  $z_k$  in the planar lattice, form the line passing through the origin and  $z_k$ , and project it back down to the cylinder to get the least coiled helix in  $\mathcal{C}$  that passes through  $(0, 0)$  and  $p_k$ . This helix is called a  $k$ -*parastichy* of the helical lattice if there are no lattice points in the line between  $(0, 0)$  and  $p_k$ . The lattice points lying in this  $k$ -parastichy form the sub-lattice  $\{(jkx, jky) \mid j \in \mathbb{Z}\}$  isomorphic to  $k\mathbb{Z}$ . Cosets of this sub-lattice are its translations by elements of  $L(x, y)$ . The parallel helices that run through these cosets are also called  $k$ -parastichies. Since the index of the sub-lattice in  $L(x, y)$  is  $k$ , there are  $k$  such  $k$ -parastichies in all.

Among the parastichies, there are two sets that we are particularly interested in, and they are the ones “most visible to the eye”. These gave rise to the study of Phyllotaxis. They correspond to parastichies formed by closest elements. In  $\Lambda(z)$ , pick the smallest lattice element with positive imaginary part. (From now on, when we say *smallest* we mean closest to the origin.) There might be several smallest, but that’s okay. Now, pick the smallest lattice point outside of the subspace spanned by the first, again with positive imaginary part. Denote the pair by  $\{z_m, z_n\}$ . It forms a basis for the planar lattice  $\Lambda(x, y)$  known as a *canonical basis* [3]. Throughout the paper  $z_m$  denotes, out of these two elements, the one with the largest argument (as complex numbers). If  $\min(|z_m|, |z_n|) < 2 \max(|z_m|, |z_n|)$ , then the  $m$ -parastichies and the  $n$ -parastichies are the most visible ones. In this case we say that  $\{z_m, z_n\}$  is a *canonical parastichy basis*

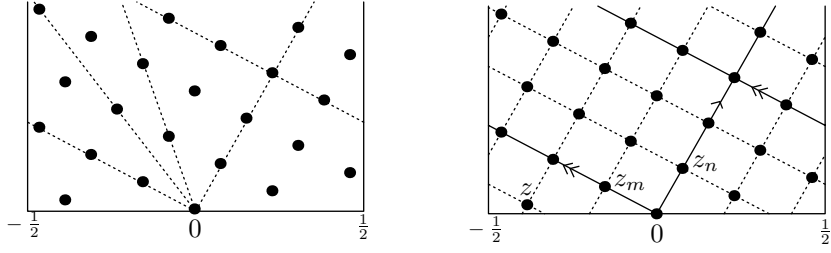


Figure 9: On the left, a helical lattice with exactly four parastichies marked as dotted lines. On the right, the same lattice with the  $m$ -parastichies and  $n$ -parastichies drawn. In this case  $m = 3$  and  $n = 5$ . Minding the identification of the two vertical edges, one can count respectively 3 and 5 parastichies.

or simply a *parastichy basis* and that the helical lattice has *parastichy numbers*  $m$  and  $n$ . When  $Re(z_m)$  and  $Re(z_n)$  are of opposite signs, the two parastichies that  $z_m$  and  $z_n$  generate wind in opposite directions. In this case, we say that the basis  $\{z_m, z_n\}$  is *opposed*<sup>1</sup>. Finally, if the canonical basis  $\{z_m, z_n\}$  is such that  $|z_m| = |z_n|$ , we say that it is a *rhombic canonical basis*. In this case we say that  $\Lambda(z)$  is a *rhombic lattice*.

## 4.2 Classification of Lattices

As we have seen above, an unrolled helical lattice generated by  $(x, y)$  gives rise to a planar lattice generated by  $z = x + iy$  and 1. Hence, the parameter space of all such planar lattices is the complex plane parameterized by  $z$ . Since  $y > 0$ , the parameter space is the upper half complex plane,  $\mathbb{H}$ , which is a model of the hyperbolic plane. Here, we will classify lattices according to their parastichy numbers. This material is a variation on a classical approach to the classification of lattices (see [3], Chapter 7, where lattices are called discrete modules, and also [17]).

### 4.2.1 The Fundamental Quadrilateral and Hexagon

We now determine the set of points  $z \in \mathbb{H}$  such that  $\{z, 1\}$  forms a canonical, rhombic canonical or parastichy basis for the lattices  $\Lambda(z)$  they generate. This serves as a template for all the regions where  $\{z_m, z_n\}$  forms such bases, as we will see in the next subsection. Define

$$Q = Q^+ \cup Q^-,$$

where

$$Q^+ = \{z \in \mathbb{H} \mid |z| \geq 1, -1/2 \leq Re(z) \leq 1/2\},$$

<sup>1</sup>Sometimes, other authors use the term “parastichy numbers” when  $\{z_m, z_n\}$  form a “conspicuous opposed parastichy pair” [1], a notion closely related but not quite equivalent to opposed canonical basis.

and  $Q^-$  is the (hyperbolic) reflection of  $Q^+$  about the unit circle centered at 0. Note that in  $Q^+$ ,  $|z| \geq 1$ , and in  $Q^-$ ,  $|z| \leq 1$ . (See Fig. 10.)

Also define  $H$  to be the region obtained by truncating the region  $Q$  above the circle of radius 2 centered at 0 and below the circle of radius  $1/2$  centered at 0.

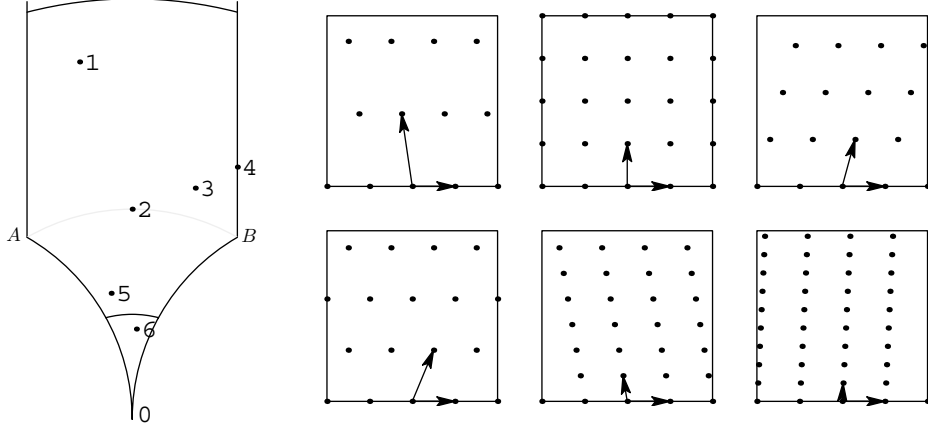


Figure 10: The regions  $Q$  and  $H$  with some of the lattices they represent, numbered 1–6, on the right. The vertices of the hyperbolic quadrilateral  $Q$  are  $\infty, A = e^{2\pi i/3}, O = (0, 0)$  and  $B = e^{\pi i/3}$ . The gray hyperbolic line inside  $Q$ , where lattice 2 is located, is an arc of the unit circle centered at  $O$  and is the set of rhombic lattices in  $Q$ . This line separates the hyperbolic triangles  $Q^+$  (above) and  $Q^-$  (below). Lattice 6 is in  $Q$  but outside  $H$ . The boxes enclosing the lattices are all the square  $[-2, 2] \times [0, 4]$ .

#### Proposition 4.1.

- (i) The pair  $\{z, 1\}$  is a canonical basis for  $\Lambda(z)$  if and only if  $z \in Q$ .
- (ii) The pair  $\{z, 1\}$  is a parastichy basis for  $\Lambda(z)$  if and only if  $z \in H$ .
- (iii) The set of rhombic lattices in  $Q$  is the arc of unit circle in  $Q$ .

Figure 10 shows the regions  $Q$  and  $H$  and some of the lattices they represent. We call  $Q$  the *fundamental quadrilateral* since it is bounded by a hyperbolic quadrilateral with vertices at  $0, \infty, A = e^{2\pi i/3}$  and  $B = e^{\pi i/3}$  ( $0$  and  $\infty$  are called *ideal vertices* since they are on the boundary of  $\mathbb{H}$ ). Likewise,  $H$  is called the *fundamental hexagon*.

*Proof.* Let  $K = \{z \in \mathbb{H} \mid \{z, 1\} \text{ is a canonical basis}\}$ ,  $K^+ = \{z \in K \mid |z| \geq 1\}$  and  $K^- = \{z \in K \mid |z| \leq 1\}$ . We now show that  $Q^+ = K^+$  and  $Q^- = K^-$ .

Suppose  $z$  is in  $Q^+$ . We want to show that  $z$  is a smallest element in  $\Lambda(z)$  outside of the sublattice  $\mathbb{Z}$  generated by 1. The following shows that  $|kz+d| > |z|$  for  $k \geq 2, d \in \mathbb{Z}$ :

$$|kz + d| \geq \text{Im}(kz + d) = \text{Im}(kz) = k|z|\text{Im}\left(\frac{z}{|z|}\right) \geq k|z|\text{Im}(A) = k|z|\frac{\sqrt{3}}{2} > |z|.$$

For the case  $k = 1$ , since  $-1/2 \leq \operatorname{Re}(z) \leq 1/2$ , it follows that  $|\operatorname{Re}(z)| \leq |\operatorname{Re}(z+d)|$  and  $\operatorname{Im}(z) = \operatorname{Im}(z+d)$ , and therefore  $|z+d| \geq |z|$ . Hence,  $z$  is a smallest element in  $\Lambda(z)$  outside of the sublattice  $\mathbb{Z}$  generated by 1 and  $\{z, 1\}$  forms a canonical basis. Since  $|z| \geq 1$ ,  $z \in K^+$ . Conversely, if  $z \in K^+$ , then we must have  $|z+d| \geq |z|$  for all  $d \in \mathbb{Z}$  and thus necessarily  $-1/2 \leq \operatorname{Re}(z) \leq 1/2$ . Hence,  $z \in Q^+$ . We have thus proven  $Q^+ = K^+$ .

We now show that  $Q^- = K^-$ . Let  $z$  be in  $K^-$ , *i.e.*,  $\{z, 1\}$  forms a canonical basis of  $\Lambda(z)$  with  $|z| \leq 1$ . Multiplying the lattice elements by  $1/z$  we obtain a lattice  $\Lambda(1/z)$  homothetic to  $\Lambda(z)$ . (Remember that, geometrically, multiplication by a complex number induces a homothety: a rotation by the argument, together with an expansion by the modulus of the complex number.) Since a homothety preserves proportions,  $\{1, 1/z\}$  is a canonical basis of  $\Lambda(1/z)$ . However  $1/z$  is in the lower half plane so we consider the mirror symmetric lattice  $\Lambda(1/\bar{z})$  generated by  $\{1, 1/\bar{z}\}$  instead. Again, this symmetry conserves proportions and thus the shortest element in the canonical basis  $\{1, 1/\bar{z}\}$  of  $\Lambda(1/\bar{z})$  is  $1/\bar{z}$ . Since  $|1/\bar{z}| \geq 1$ , we have shown that  $R(K^-) \subset K^+$ , where  $R$  is the map  $w \mapsto 1/\bar{w}$ . A parallel argument shows that  $R(K^+) \subset K^-$ . Since the map  $R$  is the well known (hyperbolic) reflection about the unit circle and  $R^2 = \operatorname{Id}$ , we conclude that  $R(K^-) = K^+$  and  $R(K^+) = K^-$ . Since by definition  $R(Q^+) = Q^-$ , and we have seen above that  $Q^+ = K^+$ , we have  $K^- = R(K^+) = R(Q^+) = Q^-$ , proving (i).

It is clear that the set of  $z \in Q$  such that  $\Lambda(z)$  is rhombic is given by the intersection of  $Q$  with the unit circle. Now, when does  $\{z, 1\}$  form a parastichy basis? For  $z \in K^+$  we need  $|z| \leq 2$  and for  $z \in K^-$  we need  $1 \leq 2|z|$ . These two conditions define two hyperbolic lines that truncate  $Q$ , lopping off its ideal vertices.  $\square$

#### 4.2.2 The Quadrilateral $Q_{mn}$ and the Hexagon $H_{mn}$

We now show that a similar homothety argument as above describes a quadrilateral region  $Q_{mn}$  and an hexagonal region  $H_{mn}$  where  $\{z_m, z_n\}$  is, respectively, a canonical and a parastichy basis of the lattice  $\Lambda(z)$ . The botanical significance of  $H_{mn}$  is that it is the region where lattices have parastichy numbers  $m, n$ .

**Proposition 4.2.** *Let  $z$  belong to the strip  $\operatorname{Re}(z) \in (0, 1)$ .*

(i) *The pair  $\{z_m, z_n\}$  is a canonical basis for  $\Lambda(z)$  oriented as  $\{z, 1\}$  if and only if*

$$z \in Q_{mn} \stackrel{\text{def}}{=} g_{mn}(Q) \quad \text{where} \quad g_{mn}(w) \stackrel{\text{def}}{=} \frac{\Delta_n w - \Delta_m}{nw - m}$$

and  $\Delta_m$  and  $\Delta_n$  are the unique integers such that

$$(*) \quad \Delta_m n - \Delta_n m = 1, \quad \left[ \frac{\Delta_n}{n}, \frac{\Delta_m}{m} \right] \subset [0, 1].$$

*In particular,  $m$  and  $n$  are always coprime.*

(ii) The pair  $\{z_m, z_n\}$  is a parastichy basis oriented as  $\{z, 1\}$  if and only if

$$z \in H_{mn} \stackrel{def}{=} g_{mn}(H).$$

(iii) Rhombic lattices of parastichy numbers  $m, n$  are in the image by  $g_{mn}$  of the rhombic lattices in  $Q$ .

Notice that statement (ii) can be rephrased as:

A lattice  $\Lambda(z)$  has parastichy numbers  $m, n$  (with  $\gcd(m, n) = 1$ ) if and only if  $z$  is in  $H_{mn}$ .

*Proof.* Assume that  $\{z_m, z_n\}$  is a canonical basis with same orientation as  $\{z, 1\}$ . In real coordinates,  $z_m = (mx - \Delta_m, my) = m(x, y) - \Delta_m(1, 0)$ , where  $\Delta_m$  is the integer closest to  $mx$ . Hence, the change of basis matrix between  $z, 1$  and  $z_m, z_n$  is

$$\begin{pmatrix} m & n \\ -\Delta_m & -\Delta_n \end{pmatrix}.$$

Since it changes integer lattice bases with same orientation, this matrix must be invertible with integer inverse, forcing its determinant to be 1:

$$(**) \quad \Delta_m n - \Delta_n m = 1.$$

Since  $\Delta_m, \Delta_n$  are integers, the above equality means that  $m$  and  $n$  must be coprime. Dividing  $(**)$  by  $mn$ , we get  $\frac{\Delta_m}{m} - \frac{\Delta_n}{n} = \frac{1}{mn}$  and in particular  $\frac{\Delta_n}{n} < \frac{\Delta_m}{m}$ .

There are countably many pairs of integers  $\Delta_m, \Delta_n$  that satisfy  $(**)$ . However, suppose  $\Delta_m + k, \Delta_n + l$  is another such pair, *i.e.*,  $(\Delta_m + k)n - (\Delta_n + l)m = 1$ . Since  $m, n$  are coprime, it is easy to check that  $k = am$  and  $l = an$  for the same integer  $a$ . In particular  $\frac{\Delta_m + k}{m} = \frac{\Delta_m}{m} + a$  and  $\frac{\Delta_n + l}{n} = \frac{\Delta_n}{n} + a$ . Since  $Re(z) \in [0, 1]$ , we must have  $Re(mz) \in [0, m]$ ,  $Re(nz) \in [0, n]$ . Since  $\Delta_m, \Delta_n$  are the closest integers to  $Re(mz), Re(nz)$ , respectively, we must have  $\Delta_m \in [0, m]$ ,  $\Delta_n \in [0, n]$ . Hence,  $\Delta_m, \Delta_n$  is the unique pair satisfying  $(*)$ .

Dividing all lattice points of  $\Lambda(z)$  by  $z_n$  gives rise to a new lattice  $\Lambda(w)$  generated by  $w = z_m/z_n$  and 1, homothetic to the lattice  $\Lambda(z)$ . Since homothety preserves proportions,  $\{w, 1\}$  must also be a canonical basis of  $\Lambda(w)$  and hence,  $w$  must belong to the fundamental quadrilateral  $Q$ . From the definition of  $z_m, z_n$ , we have  $w = \frac{mz - \Delta_m}{nz - \Delta_n}$ . This relation can easily be inverted:

$$z = \frac{\Delta_n w - \Delta_m}{nw - m} = g_{mn}(w),$$

which proves that  $z \in Q_{mn}$ .

Conversely, let  $z = g_{mn}(w) = \frac{\Delta_n w - \Delta_m}{nw - m} \in Q_{mn}$ , with  $w \in Q$  and  $\Delta_m, \Delta_n$  as in  $(*)$ . Solving for  $w$ , we get  $w = \frac{mz - \Delta_m}{nz - \Delta_n}$ . Since  $\{w, 1\}$  is a canonical basis for  $\Lambda(w)$ , if we multiply all the lattice points by the denominator  $nz - \Delta_n$ , we get a lattice generated by  $mz - \Delta_m$  and  $nz - \Delta_n$ . Since the multiplication is a homothety, the pair  $\{mz - \Delta_m, nz - \Delta_n\}$  is a canonical basis for the new

lattice. We must show that the numbers  $\Delta_m, \Delta_n$  of (\*) are in fact the closest integers to  $mx$  and  $nx$ , respectively, in order to conclude that

$$\{mz - \Delta_m, nz - \Delta_n\} = \{z_m, z_n\}.$$

Since  $\{mz - \Delta_m, nz - \Delta_n\}$  is a canonical basis,  $mz - \Delta_m$  is the closest element to 0 among  $\{mx - j\}_{j \in \mathbb{Z}}$  (and likewise for  $n$ ). Therefore,  $\Delta_m$  is the closest integer to  $mx$  (and likewise for  $n$ ). This completes the proof of (i).

A similar reasoning shows that the region where  $z_m$  and  $z_n$  form a parastichy basis is given by  $H_{mn} = g_{mn}(H)$ .  $\square$

We can define  $g_{11}(w) = \frac{1}{1-w}$  and  $Q_{11} = g_{11}(Q)$ . The quadrilateral  $Q_{11}$  is the set of lattices for which  $z$  and its translate  $z - 1$  form a parastichy basis.

The maps  $g_{mn}$ , of the form  $w \rightarrow \frac{aw+b}{cw+d}$  are *Möbius transformations*. When  $a, b, c, d$  are real and  $ad - bc > 0$ , such transformations are isometries of the hyperbolic plane  $\mathbb{H}$ , whose lines are semicircles centered on the  $x$ -axis and vertical (euclidean) half lines. In particular,  $g_{mn}$  take hyperbolic lines to hyperbolic lines and they also conserve angles between these lines. In fact,  $ad - bc = 1$  in the case of the maps  $g_{mn}$ : they form part of a subgroup of the hyperbolic isometries called  $PSL(2, \mathbb{Z})$ . Hence,  $Q_{mn}$  is congruent to  $Q$  and it is bounded by a hyperbolic quadrilateral. Similarly,  $H_{mn}$  is congruent to  $H$  and it is bounded by a hyperbolic hexagon (see Figure 11). The collection of all images of  $Q$  under the group  $PSL(2, \mathbb{Z})$  forms a tessellation of  $\mathbb{H}$  by congruent quadrilaterals, of which the  $Q_{mn}$ 's form a subset. The union of all the diagonals of the quadrilaterals  $Q_{mn}$ , which correspond to rhombic lattices of parastichy numbers  $m, n$ , together with the half line  $\mathcal{L} = \{(\frac{1}{2}, y) \mid y \geq \frac{\sqrt{3}}{6}\}$ , form a binary tree  $\mathcal{V}$  called the *van Iterson diagram* which we describe in more detail in the next section (see Figures 11 and 12).

### 4.3 Branching Points of $\mathcal{V}$

The van Iterson diagram is a binary tree. We call its vertices *branching points*. Under  $g_{mn}$ , the point  $A = e^{i2\pi/3}$  of  $Q$  (see Figure 13) maps to a branching point of  $\mathcal{V}$  and thus understanding the neighborhood of  $A_{mn} \stackrel{def}{=} g_{mn}(A)$  will help us understand  $\mathcal{V}$  and the bifurcation diagram. We define two quadrilaterals that meet  $Q$  at  $A$ :  $L$ , the image of  $Q$  under the map  $\alpha : w \mapsto w - 1$ , and  $R$  the image of  $Q$  under  $\beta : w \mapsto \frac{w}{1-w}$ . It is not hard to check that  $Q, R, L$  also meet pairwise at the edges formed by arcs of the unit circles centered at 0 and  $-1$ .

**Proposition 4.3.** *The images  $R'$  and  $L'$  of  $R$  and  $L$  under  $g_{mn}$  are*

$$R' = Q_{m, m+n} \quad \text{and} \quad L' = Q_{m+n, n}.$$

The proposition derives directly from the following lemma.

**Lemma 4.4.**  *$g_{mn} \circ \beta = g_{m, m+n}$  and  $g_{mn} \circ \alpha = g_{m+n, n}$*

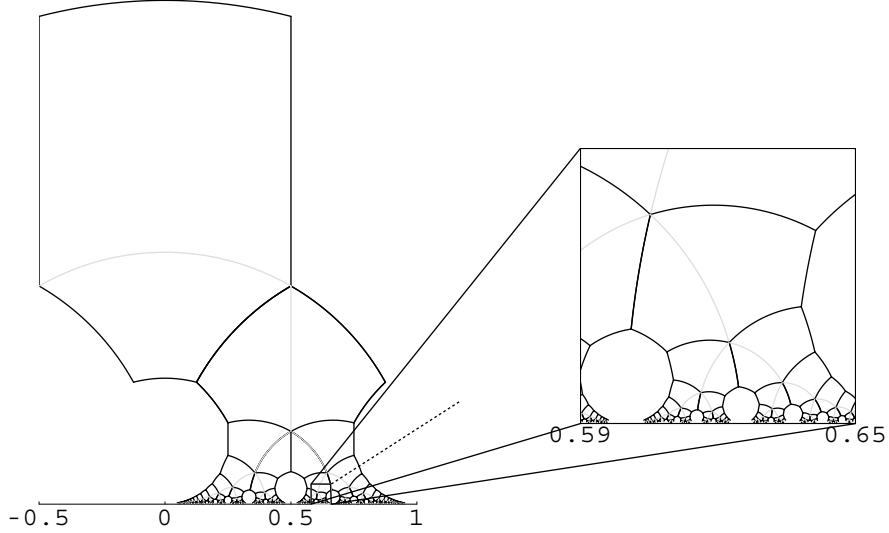


Figure 11: The hexagons (in black) and their diagonals of rhombic lattices (in grey), which form a binary tree called the van Iterson diagram. The horizontal axis is the divergence angle  $x$ , the vertical axis is the internodal distance  $y$ .

*Proof.* Using the fact that  $\Delta_m + \Delta_n = \Delta_{m+n}$  (see next Lemma) we have:

$$\begin{aligned} g_{m,n}(\beta(w)) &= \frac{\Delta_n \frac{w}{1-w} - \Delta_m}{n \frac{w}{1-w} - m} = \frac{\Delta_n w - \Delta_m + \Delta_m w}{nw - m + mw} = \\ &= \frac{(\Delta_m + \Delta_n)w - \Delta_m}{(m+n)w - m} = \frac{\Delta_{m+n}w - \Delta_m}{(m+n)w - m} = g_{m,m+n}(w). \end{aligned}$$

Therefore  $R' = g_{m+n,m}(Q) = Q_{m,m+n}$ . A similar computation shows that  $g_{mn} \circ \alpha = g_{m+n,n}$  and  $L' = Q_{m+n,n}$ .  $\square$

**Remark.** Proposition 4.3 shows that, starting at a given  $Q_{mn}$  and going down  $\mathcal{V}$  alternating between left and right branches, the indices will follow a Fibonacci-like sequence (see Subsection 5.3.2). Note also that the above lemma shows that the maps  $\alpha$  and  $\beta$  generate the maps  $g_{mn}$ . Indeed  $g_{11} = \alpha^{-1} \circ \beta$  and any other  $g_{mn}$  is obtained by composing  $g_{11}$  to the right by positive powers of  $\alpha$  and  $\beta$ . More generally, it is not hard to see that  $\alpha$  and  $\beta$  generate the whole group  $PSL(2, \mathbb{Z})$ .

We recall that the Farey sum of the two rationals  $\frac{a}{b} < \frac{c}{d}$  is the number  $\frac{a+c}{b+d}$ , and it is easily seen that  $\frac{a}{b} < \frac{a+c}{b+d} < \frac{c}{d}$ .

**Lemma 4.5.**  $\Delta_m + \Delta_n = \Delta_{m+n}$ .

*Proof.* From Proposition 4.2,

$$1 = -\Delta_n m + \Delta_m n = -\Delta_n(m+n) + (\Delta_m + \Delta_n)n \quad \text{and} \quad \left[ \frac{\Delta_n}{n}, \frac{\Delta_m}{m} \right] \subset [0, 1].$$

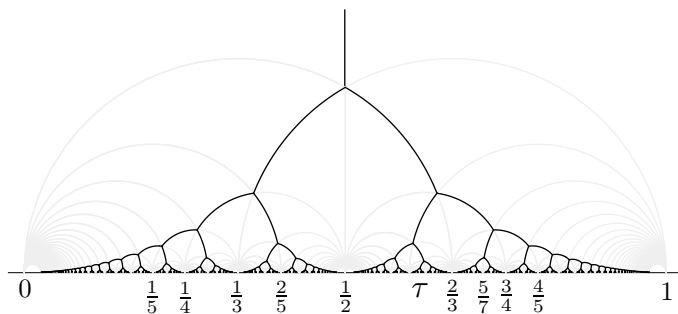


Figure 12: The van Iterson diagram, in black.

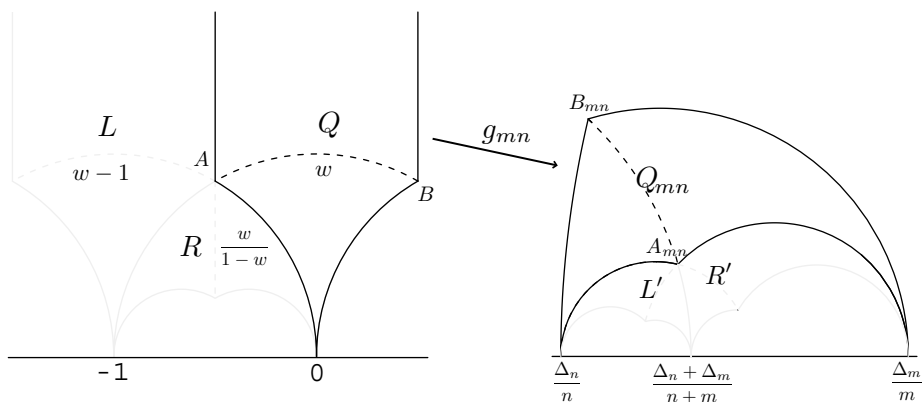


Figure 13: A quadrilateral  $Q' = Q_{mn}$  and its descendants:  $R' = Q_{m,m+n}$ ,  $L' = Q_{m+n,n}$ .

Since the Farey sum of two rationals is between them,  $[\frac{\Delta_n}{n}, \frac{\Delta_m + \Delta_n}{m+n}] \subset [\frac{\Delta_n}{n}, \frac{\Delta_m}{m}] \subset [0, 1]$ . The equation above and the uniqueness property of Proposition 4.2 applied to the pair  $m+n, n$  imply that  $\Delta_m + \Delta_n = \Delta_{m+n}$ .  $\square$

Note that the three ideal points  $0, \infty$  and  $-1$  map to  $\frac{\Delta_m}{m}, \frac{\Delta_n}{n}$  and  $\frac{\Delta_m + \Delta_n}{m+n}$  respectively. The vertices  $A = -\frac{1}{2} + i\frac{\sqrt{3}}{2}$  and  $B = \frac{1}{2} + i\frac{\sqrt{3}}{2}$  of  $Q$  are mapped to

$$\begin{aligned} A_{mn} = g_{mn}(A) &= \frac{(2n+m)\Delta_n + (2m+n)\Delta_m + i\sqrt{3}}{2(n^2 + mn + m^2)} \\ B_{mn} = g_{mn}(B) &= \frac{(2n-m)\Delta_n + (2m-n)\Delta_m + i\sqrt{3}}{2(n^2 - mn + m^2)}. \end{aligned}$$

In particular,  $Im(B_{mn}) > Im(A_{mn})$ . By Proposition 4.3,  $A_{mn} = B_{m+n,n} = B_{m,m+n}$  and so, as we travel down the branch of rhombic lattices in  $Q_{mn}$  (by letting  $y$  decrease), we encounter two branches of rhombic lattices, one in  $Q_{m+n,n}$  and one in  $Q_{m,m+n}$ . In the next section, we will see that, in the bifurcation diagram, one of these branches has one segment pruned away, leaving only one alternative as  $y$  decreases.

## 5 The Bifurcation Diagram

### 5.1 Outline

Now that we have classified lattices according to their parastichy numbers, in this section we determine the (fixed point) *bifurcation diagram* of  $\phi$ , which we denote by  $\Sigma$ . By definition, this set is formed by the points  $(x, y)$  corresponding to lattices of constant divergence angle  $x$  that are fixed points of  $\phi$  when the value of the parameter is  $y$ . Theorem 3 below shows that  $\Sigma$  is a subset of  $\mathcal{V}$ . We first introduce a few concepts.<sup>2</sup>

A *Fibonacci-like sequence*  $\{f_j\}$  is one satisfying  $f_j = f_{j-1} + f_{j-2}$ . The Fibonacci sequence  $\{F_k\}$  is the one that starts with  $F_1 = 1, F_2 = 2$ . A *noble number* is an irrational number which has a continued fraction which becomes an infinite sequence of 1's at some point. All noble numbers are images of the *golden ratio*  $\tau = \frac{-1+\sqrt{5}}{2} = 0.61803\dots$  by elements of  $PSL(2, \mathbb{Z})$  (see [12]; note that, often  $\tau$  denotes  $\frac{1+\sqrt{5}}{2} = 1.61803\dots$ ). We call a quadrilateral  $Q_{mn}$  *regular* if  $m < 2n$  and  $n < 2m$  (equivalently  $(2n - m)(2m - n) > 0$ ). Otherwise, we call it *irregular*.

For each quadrilateral  $Q_{mn}$ , we define the curve  $\sigma_{mn}$  in the following way. If  $Q_{mn}$  is regular, let  $\sigma_{mn} = \mathcal{V} \cap Q_{mn}$  (a compact curve). If  $Q_{mn}$  is irregular, let  $\sigma_{mn}$  be the segment of  $\mathcal{V} \cap Q_{mn}$  lying *strictly* between the point  $Z_{mn}$  (to be defined in Section 5.4) and  $A_{mn}$ . Now, for each *irregular* quadrilateral  $Q_{mn}$ , we also define the set  $C_{mn}$  to be the union of the curves  $\sigma_{m_i n_i}$ , where  $m_i, n_i$  are consecutive elements in the Fibonacci-like sequence starting at  $m, n$  if  $m < n$  and  $n, m$  if  $n > m$ . (See Figure 14.) As justified by Theorem 3 below, we call the sets  $C_{mn}$  *branches* of  $\Sigma$ . In particular,  $C_{12}$  and  $C_{21}$  are the Fibonacci branches.

**Theorem 3.** *The fixed point bifurcation diagram  $\Sigma$  is the disjoint union of the branches  $C_{mn}$  and the half line  $\mathcal{L} = \left\{ \left( \frac{1}{2}, y \right) \mid y \geq \frac{\sqrt{3}}{6} \right\}$ . The connected components of  $\Sigma$  are  $\mathcal{L} \cup C_{12} \cup C_{21}$  and each of the other  $C_{mn}$ 's. Each branch  $C_{mn}$  is homeomorphic to an open interval and converges to a noble number on the real axis. In particular, the Fibonacci branches  $C_{12}$  and  $C_{21}$  converge to  $\tau$  and  $1 - \tau$ , respectively.*

We will prove this theorem in the rest of this section. We will also prove that each branch  $C_{mn}$  is monotonous, in the sense that it intersects any horizontal line in at most one point. We now outline the proof. Recall that the maximin principle implies that the fixed points satisfy the following three properties:

- (p1) The parastichy basis must be rhombic.
- (p2) The parastichy basis must be opposed.
- (p3) Each element of the lattice must satisfy the global max condition for  $D$ .

---

<sup>2</sup>Note that, as we let  $y$  decrease to 0, we have to change the dimension  $N$  of the phase space. (On any given compact interval of  $y$ , a sufficiently high  $N$  can be assumed fixed, see Section 2.4.)

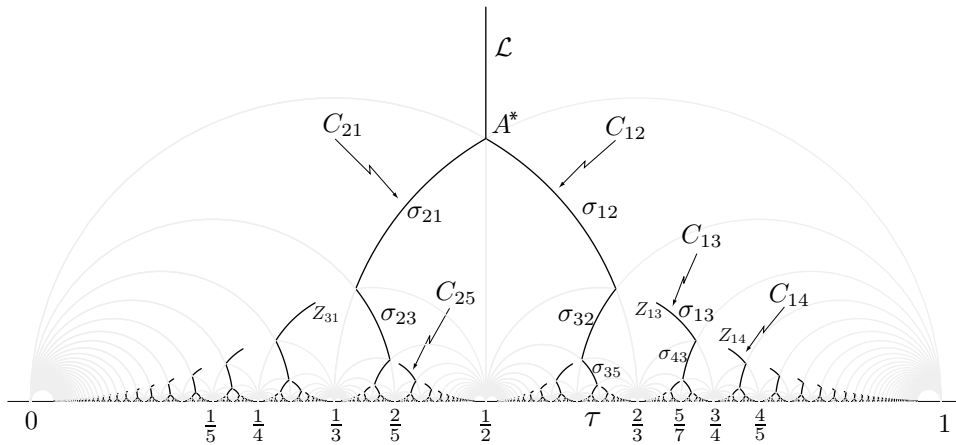


Figure 14: The bifurcation diagram  $\Sigma$ . The horizontal axis is the divergencence angle  $x$ , the vertical axis is the internodal distance  $y$ . For each irregular quadrilateral  $Q_{mn}$  there is a branch  $C_{mn}$  starting at the point  $Z_{mn}$  (see Section 5.4) winding down to the  $x$ -axis, limiting to a noble number. The segments  $\sigma_{ij}$  correspond to fixed points (lattices) with paratchy numbers  $(i, j)$ .

As we already mentioned, (p1) implies that  $\Sigma$  is a subset of the van Iterson diagram  $\mathcal{V}$ . In Section 4.3, we showed that, at each branching point of  $\mathcal{V}$ , three quadrilaterals of the form  $Q_{m+n,n}$ ,  $Q_{m,m+n}$  and  $Q_{mn}$  meet, the latter being above the former two. In Section 5.3, we show that (p2) amounts to “pruning” a segment of one of the two branches: if  $m > n$  (*resp.*  $n > m$ ), the continuous branch of opposed rhombic lattices travels from  $Q_{mn}$  to  $Q_{m,m+n}$  (*resp.*  $Q_{m+n,n}$ ) thereby choosing as indices consecutive terms in a Fibonacci-like sequence. Requiring (p3) shortens a bit more these same branches (see Section 5.4). This leaves  $\Sigma$  as a countable set of branches, each crossing a sequence of quadrilaterals with indices in a Fibonacci-like sequence.

In Section 5.5, we prove that the branches are monotonic and converge to noble numbers. We conclude in Section 5.7 by showing that, by slowly decreasing the internodal distance from a value higher than  $\frac{\sqrt{3}}{6}$  while iterating the map, the orbits shadow the fixed points of one of the main Fibonacci branches  $C_{12}$  or  $C_{21}$  which converge to  $\tau$  and  $1 - \tau$  respectively.

## 5.2 The Vertical Branch $\mathcal{L}$ of $\Sigma$

When  $y$  is large enough, only primordium  $P_1$  has influence on the position of the incoming primordium  $P_0$ , so the maximum of  $D$  occurs at the location diametrically opposed to that of  $P_1$  with divergencence angle  $\frac{1}{2}$ . Thus, any starting configuration converges, in at most  $N$  iterates, to a lattice with constant divergencence angle  $\frac{1}{2}$ , which is a fixed point. Decreasing  $y$ , the first moment when the influence of  $P_2$  is felt is when  $P_2 = P_1 + (\frac{1}{2}, y)$  and  $|P_0P_2| = |P_0P_1|$  (see

Figure 15), that is, at the point  $A^* = (\frac{1}{2}, \frac{\sqrt{3}}{6})$ . With these observations, it is easy to see that the half line  $\mathcal{L} = \left\{ (\frac{1}{2}, y) \mid y \geq \frac{\sqrt{3}}{6} \right\}$  corresponds to fixed points of the map  $\phi$ , see Figure 14. (This type of pattern, commonly seen in leaf arrangements in plants, is called *distichous*.)

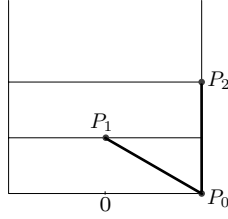


Figure 15: The first moment when  $P_2$  influences the location of the new primordium is when  $|P_0P_2| = |P_0P_1|$ . The internodal distance is  $\frac{\sqrt{3}}{6}$ .

### 5.3 Opposed Rhombic Lattices

#### 5.3.1 Regular and Irregular Quadrilaterals

For simplicity, we say that a point in  $\mathbb{H}$  is *between* two real numbers if its real part is strictly between these numbers. We refer to Section 4.3 for the definition of  $A_{mn}$  and  $B_{mn}$ .

**Lemma 5.1.** *For a given quadrilateral  $Q_{mn}$ ,*

- (i) *The vertex  $A_{mn}$  is always between the ideal vertices  $\frac{\Delta_n}{n}$  and  $\frac{\Delta_m}{m}$ .*
- (ii) *The vertex  $B_{mn}$  (and hence, all of  $Q_{mn}$ ) is between the ideal vertices  $\frac{\Delta_n}{n}$  and  $\frac{\Delta_m}{m}$  if and only if  $(2n - m)(2m - n) > 0$  (i.e., if  $Q_{mn}$  is regular).*

*Proof.*  $A_{mn}$  is between  $\frac{\Delta_n}{n}$  and  $\frac{\Delta_m}{m}$  if and only if

$$\left( \operatorname{Re}(A_{mn}) - \frac{\Delta_n}{n} \right) \left( \operatorname{Re}(A_{mn}) - \frac{\Delta_m}{m} \right) = -\frac{2m^2 + 5mn + 2n^2}{4mn(m^2 + mn + n^2)^2} < 0,$$

which is clearly always true.

On the other hand,  $B_{mn}$  is between  $\frac{\Delta_n}{n}$  and  $\frac{\Delta_m}{m}$  if and only if

$$\left( \operatorname{Re}(B_{mn}) - \frac{\Delta_n}{n} \right) \left( \operatorname{Re}(B_{mn}) - \frac{\Delta_m}{m} \right) = \frac{-(2m - n)(2n - m)}{4mn(m^2 - mn + n^2)^2} < 0$$

which is clearly equivalent to  $(2n - m)(2m - n) > 0$ . □

A given  $z \in Q_{mn}$  is between these vertices if and only if  $(x - \frac{\Delta_m}{m})(x - \frac{\Delta_n}{n}) < 0$ . This condition is equivalent to  $(mx - \Delta_m)(nx - \Delta_n) < 0$ , which means that the real parts of  $z_m, z_n$  have opposite signs, i.e.,  $\{z_m, z_n\}$  is an opposed canonical basis. We have thus proved

**Proposition 5.2.**

- (i) For a given  $z \in Q_{mn}$ ,  $z$  is between  $\frac{\Delta_n}{n}$  and  $\frac{\Delta_m}{m}$  if and only if  $\{z_m, z_n\}$  is an opposed canonical basis.
- (ii)  $Q_{mn}$  is regular if and only if all its corresponding lattices have an opposed canonical basis.
- (iii)  $Q_{mn}$  is regular if and only if it is between its ideal vertices  $\frac{\Delta_n}{n}$  and  $\frac{\Delta_m}{m}$ .

**Remark.** Proposition 5.2 part (i) includes what Adler and Jean call the Fundamental Theorem of Phyllotaxis (see [1, 15], where the term “visible opposed parastichy pair” is used instead of opposed canonical basis):

*If  $\{z_m, z_n\}$  is an opposed canonical basis, then the divergence angle  $x = \text{Re}(z)$  is in the interval  $[\frac{\Delta_n}{n}, \frac{\Delta_m}{m}]$ .*

As a direct consequence of Lemma 5.1 and Proposition 5.2 we have:

**Proposition 5.3.** *For  $(m, n) \neq (1, 1)$ , of the two quadrilaterals below  $Q_{mn}$ , one is irregular and the other regular. More specifically:*

- If  $m > n$ ,  $Q_{m, m+n}$  is regular and  $Q_{m+n, n}$  irregular.
- If  $n > m$ ,  $Q_{m, m+n}$  is irregular and  $Q_{m+n, n}$  regular.

Let us examine now the case where  $(m, n) = (1, 1)$ . The quadrilateral  $Q_{11} = g_{11}(Q)$  is regular, since it lies between its ideal vertices 0 and 1. On the other hand, since the unit circle centered at 0 is mapped to  $x = 1/2$  under the map  $g_{11}$ , the quadrilaterals  $Q_{21} = g_{11}(L)$  and  $Q_{12} = g_{11}(R)$  share an edge on  $x = \frac{1}{2} = \frac{\Delta_2}{2}$ : they are irregular.

### 5.3.2 Pruning the Tree. Fibonacci and Farey Rules

None of the points inside the diagonals of rhombic lattices of  $Q_{12}$  and  $Q_{21}$  violate (p2) (Proposition 5.2(i)). For every  $Q_{mn}$ , define  $\bar{\sigma}_{mn}$  to be the segment of opposed rhombic lattices in  $Q_{mn}$ , *i.e.*, the portion of  $\mathcal{V} \cap Q_{mn}$  which is between  $\frac{\Delta_n}{n}$  and  $\frac{\Delta_m}{m}$ . If  $Q_{mn}$  is regular, then  $\bar{\sigma}_{mn}$  is all of  $\mathcal{V} \cap Q_{mn}$ , thus in this case  $\bar{\sigma}_{mn} = \sigma_{mn}$  (as defined before Theorem 3). If  $Q_{mn}$  is irregular,  $\bar{\sigma}_{mn}$  is disconnected from the vertex  $B_{mn}$  (see Figure 16). This, together with Lemma 4.5 and Propositions 5.2 and 5.3 implies the following general rules:

**Proposition 5.4 (Fibonacci & Farey Rules).** *Suppose  $m > n$  (a similar statement holds for  $n > m$ ). At the branching point  $A_{mn}$ ,  $\bar{\sigma}_{mn}$  is connected to  $\bar{\sigma}_{m, m+n}$  and not to  $\bar{\sigma}_{m+n, n}$ . Hence, decreasing the parameter  $y$  produces a transition of parastichy numbers from  $(m, n)$  to  $(m, m+n)$ .*

*The divergence angles of the lattices in  $\bar{\sigma}_{mn}$  lie in the interval  $[\frac{\Delta_n}{n}, \frac{\Delta_m}{m}]$ , those of  $\bar{\sigma}_{m, m+n}$  lie in  $[\frac{\Delta_m + \Delta_n}{m+n}, \frac{\Delta_m}{m}]$ .*

Thus, the set of opposed rhombic lattices is a union of branches starting at irregular quadrilaterals and zigzagging down through regular quadrilaterals following Fibonacci-like sequences. We will see in the next section that the segments  $\bar{\sigma}_{mn}$  are further shortened by requiring the rule (p3) of global maximization of  $F$ .

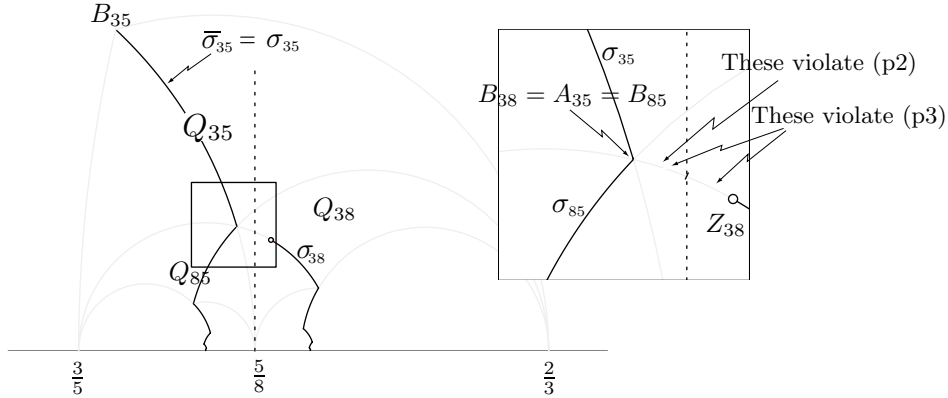


Figure 16: Pruning the van Iterson tree. In the regular quadrilaterals the whole diagonal of rhombic lattices consists of fixed points, and so forms part of the bifurcation diagram  $\Sigma$  ( $\sigma_{35}$  and  $\sigma_{85}$  in the figure) (see Section 5.4). However, in the irregular quadrilaterals a segment of it violates property (p2) (Proposition 5.2(i)) and a larger segment violates property (p3) (see Section 5.4). The remaining segment of this diagonal ( $\sigma_{38}$  in the figure, which does not include the point  $Z_{38}$ ) is in  $\Sigma$ .

#### 5.4 Further Pruning: Requiring Global Maximum for $D$

We turn to property (p3): each element of a lattice must satisfy the global maximum condition for  $D$  in order for the lattice to be a fixed point of the map  $\phi$ . The reader may have remarked that for some configurations the map  $\Phi$  is not well defined: there may be more than one point on the edge of the apical meristem  $\mathbb{S}^1 \times \{0\}$  that maximizes  $D(p)$ . These configurations—where  $F$  is multivalued—are rare (codimension 1), but are important as they mark starting points for branches of the fixed point bifurcation diagram  $\Sigma$ . We shall now determine those lattices  $\Lambda(z)$  with rhombic opposed parastichy bases (i.e., satisfying properties (p1) and (p2)) for which property (p3) holds, making them fixed points of  $\phi$ .

We have seen in Section 5.2 that the vertical half-line  $\mathcal{L}$  consists of fixed points. We now consider a lattice  $\Lambda(z)$  in  $Q_{mn}$ ,  $(m, n) \neq (1, 1)$ , with rhombic opposed parastichy basis  $\{z_m, z_n\}$ . The partition of  $\mathcal{C}$  into regions of points that are closer to one particular lattice point than to any other forms a collection of *Voronoi cells*. For our lattice, we take such a partition of  $\mathcal{C}$  without including the point  $z_0 = 0$  (see Fig. 17). The boundary between two adjacent Voronoi cells is a segment of the perpendicular bisector for the two lattice points that generate the two cells. We call the set  $T$  of Voronoi cells in the partition that intersect  $\mathbb{S}^1 \times \{0\}$  the *first tier*. The Voronoi cell generated by  $z_k$  is denoted by  $V_k$ . Let  $p = \max\{m, n\}$  and  $q = \min\{m, n\}$ .

**Proposition 5.5.** *In a rhombic lattice, all of the maxima of the function  $D$  occur in the boundary of  $V_p$ .*

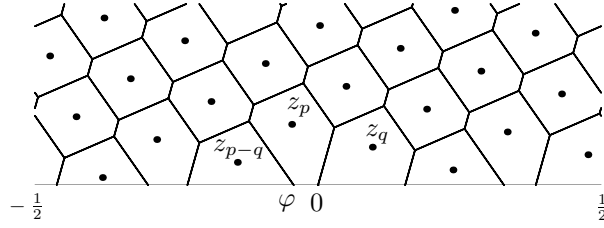


Figure 17: The partition of  $\mathcal{C}$  into regions that are closer to one particular lattice point than to any other forms a collection of *Voronoi cells*. The boundaries are segments of the perpendicular bisectors between lattice points. If the lattice is rhombic, as in the figure, the origin is on the boundary of the cell  $V_p$  generated by  $z_p$ .

The proof is in Appendix II.

The lattice point  $z_0 = 0$  is at the intersection of the common boundary of  $V_p$  and  $V_q$  with  $\mathbb{S}^1 \times \{0\}$ . Let  $\varphi$  be the intersection point on the common boundary of  $V_p$  and  $V_{p-q}$  (see Figure 17). The distances to  $z_p$  of these points are  $D(0)$  and  $D(\varphi)$ .

By Proposition 5.5, one or both of these is the maximum of  $D$ . With simple geometry and algebra, and using the fact that  $\delta_{p-q} = \delta_p - \delta_q$  (see Lemma 4.5),

$$\varphi = \frac{|z_p|^2 - |z_{p-q}|^2}{2\delta_q}.$$

$D(0) > D(\varphi)$  when  $\delta_p = \operatorname{Re}(z_p)$  is further from 0 than it is from  $\varphi$ . That is, when

$$\delta_p^2 > \left( \delta_p - \frac{|z_p|^2 - |z_{p-q}|^2}{2\delta_q} \right)^2.$$

This is equivalent to  $4\delta_p\delta_q < |z_p|^2 - |z_{p-q}|^2$ . If we substitute  $|z_p|^2 = \delta_p^2 + (py)^2$ ,  $|z_{p-q}|^2 = (\delta_p - \delta_q)^2 + (p-q)^2y^2$ ,  $\delta_p = px - \Delta_p$  and  $\delta_q = qx - \Delta_q$ , we get

$$D(0) > D(\varphi) \iff \left( x - \frac{\Delta_q}{q} \right) \left( x - \frac{2\Delta_p + \Delta_q}{2p+q} \right) < \frac{2p-q}{2p+q} y^2, \quad (1)$$

which is a region bounded by a hyperbola. Recall that the diagonal of rhombic lattices ( $\bar{\sigma}_{mn}$ ) is part of the circle  $|z_m| = |z_n|$ . The single intersection point (in  $\mathbb{H}$ ) of this circle and the hyperbola is

$$Z_{mn} = \frac{m(2\Delta_m + \Delta_n) - n(2\Delta_n + \Delta_m)}{2(m^2 - n^2)} + i \frac{\sqrt{3}}{2|m^2 - n^2|}.$$

Notice that the expression is symmetric in  $m$  and  $n$ , so this is the expression for  $Z_{mn}$  in both cases,  $p = m$  and  $p = n$ .

**Lemma 5.6.** *The point  $Z_{mn}$  lies in  $\bar{\sigma}_{mn} \subset Q_{mn}$  if and only if  $Q_{mn}$  is an irregular quadrilateral.*

*Proof.* The point  $Z_{mn}$  lies in  $\bar{\sigma}_{mn}$  if it is between  $\operatorname{Re}(A_{mn})$  and  $\operatorname{Re}(B_{mn})$ , which is true if and only if

$$(\operatorname{Re}(A_{mn}) - \operatorname{Re}(Z_{mn}))(\operatorname{Re}(B_{mn}) - \operatorname{Re}(Z_{mn})) = \frac{3mn(2m-n)(2n-m)}{4(n^4 + m^2n^2 + m^4)(m^2 - n^2)^2} \leq 0,$$

which is equivalent to  $(2m - n)(2n - m) \leq 0$ , *i.e.*,  $Q_{mn}$  is irregular.  $\square$

**Remark.**  $A^* = B_{12} = B_{21} = Z_{12} = Z_{21}$ .

**Lemma 5.7.** *For the lattice corresponding to  $A_{mn}$ ,  $D(0) > D(\varphi)$ .*

*Proof.* One can check by direct substitution if  $A_{mn}$  is in the region where (1) holds. One can also see it this way: the point  $A$  in  $Q$  lies on the hyperbolic line  $x = -1/2$  whose ideal points are  $-1/2$  and  $\infty$ , and also on the hyperbolic line whose ideal points are 0 and  $-2$ . Therefore, applying the map  $g_{mn}$ , we get that  $A_{mn}$  lies on the hyperbolic lines (euclidean circles) whose ideal points are  $\frac{2\Delta_m + \Delta_n}{2m+n}$  and  $\frac{\Delta_n}{n}$  for one line, and  $\frac{2\Delta_n + \Delta_m}{2n+m}$  and  $\frac{\Delta_m}{m}$  for the other line. The equations are

$$\begin{aligned} 0 &= y^2 + \left(x - \frac{\Delta_n}{n}\right) \left(x - \frac{2\Delta_m + \Delta_n}{2m+n}\right) \quad \text{and} \\ 0 &= y^2 + \left(x - \frac{\Delta_m}{m}\right) \left(x - \frac{2\Delta_n + \Delta_m}{2n+m}\right). \end{aligned}$$

In either case ( $p = m$  or  $p = n$ ) the left hand side of the second inequality of (1) is equal to  $-y^2$ , making the inequality obviously true. Hence, for the lattice  $\Lambda(A_{mn})$ , the point  $z_p$  is further from 0 than it is from  $\varphi$ .  $\square$

Now, as we move  $z$  up from  $A_{mn}$  along  $\bar{\sigma}_{mn}$  towards  $B_{mn}$ , the position of  $\varphi$  moves continuously. As long as  $z$  doesn't cross  $Z_{mn}$ ,  $D(0) > D(\varphi)$ , so condition (p3) is satisfied and the lattice is a fixed point of  $\phi$ . If  $Q_{mn}$  is regular, then  $Z_{mn}$  is not in  $\bar{\sigma}_{mn}$  and all of  $\bar{\sigma}_{mn} = \sigma_{mn}$  corresponds to fixed points. If  $Q_{mn}$  is irregular, then  $Z_{mn}$  is in  $\bar{\sigma}_{mn}$  and the only points in  $Q_{mn}$  corresponding to fixed points are those on  $\bar{\sigma}_{mn}$  strictly between  $Z_{mn}$  and  $A_{mn}$ . Since in the irregular case this segment of  $\bar{\sigma}_{mn}$  is  $\sigma_{mn}$ , we have proved

**Theorem 4.** *In all quadrilaterals  $Q_{mn}$ , the curves  $\sigma_{mn}$  correspond to fixed points of the map  $\phi$  and there are no other fixed points in  $Q_{mn}$ .*

Continuing the proof of Theorem 3, recall that the branches  $C_{mn}$  are unions of curves  $\sigma_{m_i n_i}$ . By Proposition 5.4 and Theorem 4, the curves  $C_{mn}$  are homeomorphic to open intervals and consist of fixed points. We now need to show that any fixed point not in  $\mathcal{L}$  belongs to some  $C_{mn}$ . Since the quadrilaterals  $Q_{mn}$  tessellate the set of all cylindrical lattices, it suffices to show that every curve  $\sigma_{kl}$  is included in some branch  $C_{mn}$ . Assume  $k < l$  and start building a Fibonacci-like sequence backwards by subtraction:  $\dots, i, j, \dots, 2k - l, l - k, k, l$ . The curve  $\sigma_{kl}$  is connected to all the curves  $\sigma_{ij}$ , by Proposition 5.4. Stop the process when the sequence becomes negative. Thus, at some step  $m, n$ , with say  $m < n$ , we have  $2m - n \leq 0$ , *i.e.*, the sequence of  $\sigma$ 's enters an irregular quadrilateral  $Q_{mn}$ . (Note that  $1 = \gcd(k, l) = \gcd(m, n)$ .) We have proven that  $\Sigma$  is the union of the branches  $C_{mn}$  and  $\mathcal{L}$ .

## 5.5 Limits to Noble Numbers. End of Proof of Theorem 3

From Proposition 5.4, the Fibonacci branch  $C_{21}$  starting in  $Q_{21}$ , visits the sequence of quadrilaterals  $Q_{21}, Q_{23}, Q_{53}, Q_{58}, Q_{13,8}, \dots, Q_{m_k, n_k}, \dots$  with corresponding intervals  $[\frac{\Delta_{n_k}}{n_k}, \frac{\Delta_{m_k}}{m_k}]$ :  $[0, \frac{1}{2}], [\frac{1}{3}, \frac{1}{2}], [\frac{1}{3}, \frac{2}{5}], [\frac{3}{8}, \frac{2}{5}], [\frac{3}{8}, \frac{5}{13}], \dots$ . In particular, this Fibonacci branch converges on the real axis to

$$\lim_{n \rightarrow \infty} \frac{F_{n-2}}{F_n} = \lim_{n \rightarrow \infty} \left(1 - \frac{F_{n-1}}{F_n}\right) = 1 - \tau.$$

The last equality makes use of the well known fact that  $\lim_{n \rightarrow \infty} \frac{F_{n-1}}{F_n} = \tau$ .

We now turn to an arbitrary branch  $C_{mn}$  of  $\Sigma$ .

Lemma 4.4 implies that for any two quadrilaterals  $Q_{mn}$  and  $Q_{m'n'}$ , we have  $Q_{m'n'} = f(Q_{mn})$  where  $f = g_{m'n'} \circ g_{mn}^{-1} \in PSL(2, \mathbb{Z})$ . Moreover, for any finite word

$$\omega = \beta^{k_1} \circ \alpha^{k_1} \circ \dots \circ \beta^{k_p} \circ \alpha^{k_p}$$

on  $\alpha, \beta$ , the two quadrilaterals  $K$  and  $K'$  below  $Q_{mn}$  and  $Q_{m'n'}$  obtained by  $K = g_{mn} \circ w(Q)$  and  $K' = g_{m'n'} \circ w(Q)$  satisfy  $f(K) = f \circ g_{mn} \circ w(Q) = K'$ . In particular, the sequence of quadrilaterals that a branch  $C_{mn}$  traverses is  $g_{mn} \circ w_j(Q)$  where  $w_j$  are words with alternating  $\alpha$  and  $\beta$ . By continuity the limit point of  $C_{mn}$  is noble, since it is the image of  $\tau$  (which is the endpoint of  $C_{12}$ ) by  $g_{mn} \circ g_{12}^{-1} \in PSL(2, \mathbb{Z})$ .

This concludes the proof of Theorem 3.

## 5.6 Monotonicity of Branches

We show here that all the branches  $C_{mn}$  in the bifurcation diagram are *monotonic* in the sense that they are graphs over the  $y$  axis. Denote  $O = g_{mn}(-1)$  and let  $C$  be the point of intersection of the hyperbolic line  $l$  through  $O, A_{mn}$  and  $B_{mn}$  with either of the vertical lines  $x = \frac{\Delta_m}{m}$  or  $x = \frac{\Delta_n}{n}$ . The segment of  $l$  between  $A_{mn}$  and  $B_{mn}$  is  $\bar{\sigma}_{mn}$ .

**Lemma 5.8.** *Assume that  $(m, n) \neq (1, 1)$  are relatively prime. The hyperbolic line segment  $OC$  of  $l$  is monotonic.*

*Proof.* It suffices to show that the point  $M$  of highest imaginary part in the (hyperbolic) line  $l$  is *not* between  $\frac{\Delta_n}{n}$  and  $\frac{\Delta_m}{m}$ . The real part of  $M$  is the midpoint between the two ideal vertices of  $l$ :  $O = \frac{\Delta_m + \Delta_n}{m+n}$  and  $g_{mn}(1) = \frac{\Delta_m - \Delta_n}{m-n}$ . Hence,  $Re(M) = \frac{\Delta_m m - \Delta_n n}{m^2 - n^2}$  and  $M$  is outside of  $\frac{\Delta_n}{n}$  and  $\frac{\Delta_m}{m}$  if and only if

$$\left(\frac{\Delta_m m - \Delta_n n}{m^2 - n^2} - \frac{\Delta_m}{m}\right) \left(\frac{\Delta_m m - \Delta_n n}{m^2 - n^2} - \frac{\Delta_n}{n}\right) = \frac{1}{(m^2 - n^2)^2} > 0,$$

which is clearly always true (since  $m \neq n$ ).  $\square$

**Corollary 5.9.** *All branches  $C_{mn}$  of  $\Sigma$  are monotonic.*

*Proof.* The branches  $C_{mn}$  are made of segments  $\bar{\sigma}_{m_i n_i}$ . Whether  $Q_{m_i n_i}$  is regular or not, these segments are all contained in segments of the type  $OC$  as above.  $\square$

## 5.7 A Scenario for Fibonacci Phyllotaxis

Many quantitative botanical studies document the change of internodal distance as a plant grows. (In other geometries, other parameters than the internodal distance may be used to a similar effect. For the flat disk, one commonly uses as an equivalent parameter the ratio between the radial distances of two successive primordia to the center of the apex, called the plastochrone ratio.) This is especially marked when the plant makes a transition between the vegetative mode to the inflorescence mode (see *e.g.*, [20]). The scenario that we explore now with our model assumes that internodal distance decreases slowly from a relatively high value ( $y > \frac{\sqrt{3}}{6}$ ) while the iterative process is running. The guiding principle is given by the stability of all fixed points: it insures that a configuration sufficiently close to a fixed point on a branch  $C_{mn}$  of  $\Sigma$  will remain in the basin of attraction of fixed points of  $C_{mn}$  with slightly lower  $y$  values. Hence, starting with a configuration near  $C_{mn}$ , and slowly decreasing  $y$  while iterating  $\phi$ , we obtain orbits that follow closely the branch  $C_{mn}$ .

As argued in section 5.3.2, at high internodal distances  $y > \frac{\sqrt{3}}{6}$ , all configurations tend quickly to the lattice  $\Lambda(\frac{1}{2}, y)$  in the vertical half-line of  $\Sigma$ , forming a distichous pattern. At the point  $A^* = (\frac{1}{2}, \frac{\sqrt{3}}{6})$ , there is a transition from distichous ( $\mathcal{L}$ ) to spiral phyllotaxis ( $C_{12}$  or  $C_{21}$ ) (see Figure 14). In particular the symmetry of the distichous patterns (divergence angle of  $180^\circ$ ) is broken at this point. Note however that this bifurcation is not of a common type in Dynamical Systems: the map  $\phi$  is not differentiable at the configuration corresponding to  $A^*$  because it is multivalued on  $x = 1/2$  immediately below  $A^*$ . Decreasing  $y$ , the choice of  $C_{12}$  or  $C_{21}$  below  $A^*$  locks the pattern in a certain winding direction (*chirality*). From then on, decreasing  $y$  slowly, the iterated configurations stay close to the fixed points in the Fibonacci branch chosen. They thus exhibit increasing Fibonacci parastichy numbers and divergence angles increasingly close to  $360^\circ(\tau) = 222.492\dots$ , or  $360^\circ(1 - \tau) = 137.507\dots$

Starting at values of  $y$  lower than  $\frac{\sqrt{3}}{6}$  and/or decreasing  $y$  erratically may yield patterns in the other branches of the bifurcation diagram. Interestingly, the ones most observed in nature after the Fibonacci branches are the Lucas branches  $C_{13}$  or  $C_{31}$ , following the Lucas sequence  $1, 3, 4, 7, \dots$ : these branches are the largest ones after the Fibonacci branches, and they are also close to them in the parameter space.

## 6 Periodic Orbits

Stable patterns other than lattices can occur. Indeed, in research still in progress [4], we found periodic orbits for the map  $\phi$ , *i.e.*, configurations  $\{x_0, x_1, \dots, x_{N-1}\}$  with  $x_{k+j} = x_k$  for all  $k$  and some period  $j$ . Our first investigations were numerical and performed in a *centric* model where the geometry of the apex is assumed to be that of a flat disk. One of the periodic orbits we found is of period 8 and, expressed in degrees rounded to the nearest integer is:  $\{130^\circ, 89^\circ, 89^\circ, 130^\circ, 89^\circ, 89^\circ, 130^\circ, 315^\circ, 130^\circ, \dots\}$ . This remarkably coincides with

measurements made by Tucker [29] on a magnolia carpel:  $\{134^\circ, 94^\circ, 83^\circ, 138^\circ, 92^\circ, 86^\circ, 136^\circ, 310^\circ, 134^\circ, \dots\}$ . This phenomenon may be more prevalent than realized because the phyllotactic patterns produced by periodic divergence angles can look superficially like a spiral lattice. Only close scrutiny (*e.g.*, [29]) can reveal the periodicity of the divergence angles in such plant patterns.

Questions that we are investigating include: Are all periodic orbits stable? If so, do their basins of attraction entirely fill the intersections of the domains of the iterates of  $\phi$ ? If not, are there chaotic orbits?

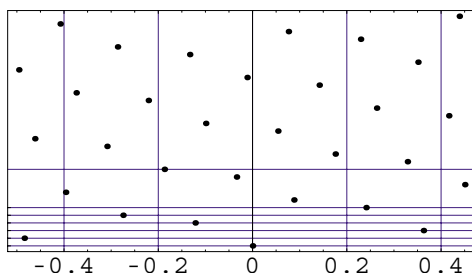


Figure 18: A double lattice configuration corresponding to a period two orbit. The internodal distance is  $y = 0.0162374568$ , and the divergence angle alternates between  $\alpha = 0.515688$  and  $\beta = 0.846893$ . The existence and stability of this orbit was rigorously proven using interval arithmetics in Longhi [19]. Contrary to Douady and Couder’s observations [7], the angles  $\alpha$  and  $\beta$  are not simply rationally related.

## 7 Comparison with Other Works

The process of building a mathematical model for meristematic development has spanned the last two centuries. An important step was taken by the Bravais brothers [5] who showed that when the divergence angle is close to the golden angle then the parastichy numbers are consecutive Fibonacci numbers. One of the first botanists to study meristematic development under the microscope was Hofmeister [13]. His observations led him to hypothesize that when a single primordium forms it always does so in the least crowded spot along the apical ring. While Hofmeister’s hypothesis is simple enough to state, it is not so easy to see what types of patterns can form from it. Many people thought that his hypothesis was incompatible with the idea that the divergence angle is always close to the golden angle.

The complete mechanism of primordia formation remains unknown. In 1913 Schoute [23] proposed that existing primordia inhibit the production of new primordia through a chemical inhibitor. Later Turing [30] constructed one of the first reaction–diffusion equations to model development. Even though his approach has become popular in developmental biology, he didn’t achieve his goal of obtaining phyllotactic patterns. With the advent of computers, Veen [31] implemented Hofmeister’s hypothesis with a cellular automata like program

based on a reaction–diffusion model. He obtained phyllotactic patterns with a divergence angle close to the golden angle. Unfortunately, computers weren’t very powerful in those days. The angular resolution in Veen’s program was only about  $10^\circ$  and it did not receive a lot of attention. In subsequent years others ([24, 28, 32]) performed computer simulations with reaction–diffusion equations to model meristematic development but achieved limited success.

In 1992 the physicists Douady and Couder took a new approach implementing Hofmeister’s hypothesis. They represented the primordia with particles which exerted a repulsive force towards each other. They did this using both computer simulations and a physical model that used magnetized oil droplets. They were quite successful and left little doubt that Hofmeister’s hypothesis could indeed lead to the golden angle. Afterwards, Meinhardt *et. al.* [21] were able to obtain similar results with reaction–diffusion equations (whether meristematic development is guided by chemical reactions or by mechanical stresses as Green [11] proposed is still an open question).

A rigorous analysis such as presented in this paper is extremely difficult to do with PDE models. Moreover, as mentioned earlier, there is no agreement among botanists on the biophysical mechanisms of primordium formation. Nonetheless, it would be interesting to show that in some sense our system appears as a discretization of some of the PDE’s that have been proposed.

As mentioned in the introduction, our approach bears the most in common with the work of Kunz [16]. The main difference between his system and ours is his implementation of the inhibitory field between primordia. He assumes that *all* primordia act on the nascent one, which must therefore minimize an inhibiting energy of the form:

$$W(p) = \sum_{k=1}^N U(\|P_k - p\|),$$

where  $U(x)$  is a positive decreasing function of  $x$ . Our approach is equivalent to using an inhibiting energy of the form:

$$X(p) = \sup_k U(\|P_k - p\|),$$

which can be seen as keeping only the largest term in the sum defining  $W$ . These two inhibitory fields correspond to two extreme possibilities. With the field  $X$ , a point on the apical ring only “feels” the inhibition produced by the primordium nearest to it. With the field  $W$ , a point on the apical ring “feels” the inhibition produced by all of the primordia. Most likely, in nature a point on the apical ring “feels” the inhibition produced by some but not all of the primordia. Fortunately, as shown by Hotton [14], when  $U(x) = x^{-s}$  and  $s$  is sufficiently large, there is no qualitative difference between the fixed points saga for a dynamical system using  $W$  and our present definition using the maximin principle. Kunz has similar, less complete, asymptotic results, where he shows that the bifurcation diagram of his system is contained within certain regions tending to noble numbers.

Whereas Kunz’s model does not allow the use of hyperbolic geometry, Levitov [17, 18] brought it in very nicely in his study of a problem which is in a sense dual to ours. He considered only lattices with divergence angle, say  $x$ , and minimized the energy:

$$E(x) = \sum U(\|P_k(x)\|),$$

where  $U$  is as above and  $P_k(x) = (\delta_k, ky)$  is the  $k$ -th primordium in the lattice  $\Lambda(x, y)$ . Therefore, minimizing  $E$  answers the question: for a fixed internodal distance, which lattice exerts the least inhibition on the origin? It turns out that the answer to this question yields, varying the internodal distance, a critical point bifurcation diagram remarkably similar to ours. In fact, keeping only the largest term in  $E$  yields a maximin principle, whose critical bifurcation diagram is the subset of the van Iterson diagram one obtains by requiring properties p1 and p2 (but not p3). This is, in essence, what Adler [2] did and, as in this paper, the simplification to a maximin principle allows complete rigor (Adler used only simple Euclidean geometry techniques). In other words, Adler’s model bears a similar relation to Levitov’s that ours does to Kunz’s.<sup>3</sup> The limitation with the approaches of Adler and Levitov is that they are not dynamical and, moreover, they assume that the patterns are lattices in the first place. Douady [6] analyzed Hofmeister’s model in terms of disk packing. He arrived at a diagram of “solutions” which is geometrically the same as our bifurcation diagram, including the starting points  $Z_{mn}$  for the branches. He implicitly left open the possibility that there could have been other places where the branches should be pruned.

It is important to remark that Douady and Couder ([8, 9]) moved on from a model based on the Hofmeister hypotheses to one based on hypotheses proposed by the botanists Snow and Snow [27], namely that primordia form *when and where* the inhibitory field is small enough. This threshold model can also lead to a dynamical system, which Kunz [16] investigates somewhat (see also [6] for some mathematical, although not dynamical, exploration of the model in its “spiral” mode). Douady and Couder’s computer simulations show that a model using the Snow’s hypothesis has the big advantage of giving rise to *whorl patterns* where several primordia are born at essentially the same time and are spread out equally around the circumference of the apex. One can conceive of the model based on the Hofmeister hypotheses as a “submode” of the model based on Snows’ hypotheses.

It is possible that there is a relationship between whorl patterns and periodic orbits. As Douady & Couder [9] point out, a whorl pattern can continuously deform to a regular spiral lattice pattern. At intermediate stages of such a deformation there is periodicity in both the vertical and angular positions of primordia.

---

<sup>3</sup>This answers a question posed by Adler in [2] as to the relationship between these different models.

## 8 Appendix I: Proof of Theorem 2

*Proof.* We choose to work in the absolute angles coordinates here. See [14] for a proof in divergence angle coordinates. Remember that  $S \circ \Phi = \phi \circ S$ .  $\text{Ker}S = \text{Span}\{(1, 1, \dots, 1)\}$  is a subset of the 1-eigenspace for  $D\Phi$ : this general fact about symmetry can be seen directly in the matrix  $D\Phi$  below. Moreover, if  $v$  is a  $\lambda$ -eigenvector for  $D\Phi$  then  $DSv$  is a  $\lambda$ -eigenvector for  $D\phi$ . Hence, the spectrum of  $D\Phi$  is just the union of  $\{1\}$  and the spectrum of  $D\phi$ . In other words, if we show that  $D\Phi$  has 1 as a simple eigenvalue and that all other eigenvalues have modulus strictly less than 1, then the spectrum of  $D\phi$  is inside the open unit disk—which would prove the stability of fixed points of  $\phi$ .

To compute  $D\Phi$ , first note that, for all  $k > 0$ ,  $\partial X_k / \partial x_j = 0$  if  $j \neq k - 1$ , and  $\partial X_k / \partial x_{k-1} = 1$ . The interesting part of the computation lies in the first row. Remember that the two nearest neighbors, say  $P_m$  and  $P_n$ , of the incoming primordium  $P_0$  must lay on opposite sides of it. Moreover,  $P_0$  lays at the intersection of the circle  $\mathbb{S}^1 \times \{0\}$  and the perpendicular bisector of  $P_n$  and  $P_m$ . Using the coordinates  $P_n = (\Theta_n, Y_n) = (\theta_{n-1}, Y_n)$ ,  $P_m = (\Theta_m, Y_m) = (\theta_{m-1}, Y_m)$ ,  $P_0 = (\Theta_0, 0)$ , simple algebra gives:

$$\Theta_0 = \frac{1}{2} \left[ \frac{Y_m^2 - Y_n^2}{\theta_{m-1} - \theta_{n-1}} + \theta_{n-1} + \theta_{m-1} \right]. \quad (1)$$

Note that  $Y_n = y_n + y = (n + 1)y$  and  $Y_m = (m + 1)y$  are constants here. Hence, for all  $k \neq m, n$ ,  $\frac{\partial \Theta_0}{\partial \theta_k} = 0$ , as expected. Furthermore:

$$a \stackrel{\text{def}}{=} \frac{\partial \Theta_0}{\partial \theta_{n-1}} = \frac{1}{2} \left[ \frac{Y_m^2 - Y_n^2}{(\theta_{m-1} - \theta_{n-1})^2} + 1 \right].$$

The same computation yields  $\frac{\partial \Theta_0}{\partial \theta_{m-1}} = 1 - a$ .

**Lemma 8.1.**  $a \in (0, 1)$ .

*Proof.* This is a consequence of the fact that  $P_n$  and  $P_m$  must lay on opposite sides of  $P_0$ . Say  $\theta_{n-1} < \Theta_0 < \theta_{m-1}$ . Using Equation (1) and some elementary algebra:

$$\theta_{n-1} < \Theta_0 < \theta_{m-1} \iff 0 < \frac{Y_m^2 - Y_n^2}{(\theta_{m-1} - \theta_{n-1})^2} + 1 < 2 \iff 0 < 2a < 2,$$

which proves the lemma.  $\square$

Hence, the differential of  $\Phi$  is:



$\min\{m, n\}$ . If we are at a triple point, there are three lattice points  $z_{k_i}$  ( $k_i > 0$ ) equally close to the origin  $z_0 = 0$ , we let  $p$  be the largest of these three indices and  $q$  the second largest. It is a general fact about Voronoi cells of complete planar lattices that they are all congruent (by homogeneity of the lattice). The boundaries are made of perpendicular bisectors of pair of points in the lattice. It is well known that for a given point  $z_k$ , it suffices to consider bisectors with the eight neighbors  $z_k \pm z_p, z_k \pm z_q, z_k \pm z_{p-q}$  and  $z_k \pm z_{p+q}$ . We denote these eight neighbors by  $N_p, N_{-p}, N_q, N_{-q}, N_{p-q}, N_{-(p-q)}, N_{p+q}$  and  $N_{-(p+q)}$ , and the corresponding bisectors by  $B_p, B_{-p}, B_q$ , etc. (see Figure 19). Notice that

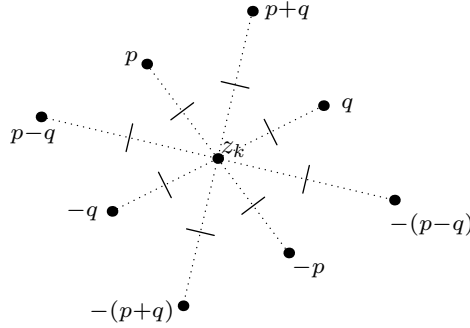


Figure 19: The lattice point  $z_k$  and its eight neighbors  $N_p, N_q, N_{-p}, \dots$ . Segments of the corresponding bisectors  $B_p, B_q, B_{-p}, \dots$  are also depicted.

$B_x$  and  $B_{-x}$ ,  $x = p, q, p + q, p - q$ , are parallel. Since  $\{z_p, z_q\}$  is a canonical basis, the boundaries of a general cell  $V_k$  are segments of  $B_p, B_q, B_{-p}, B_{-q}$  and, in general, either segments of the pair  $B_{(p+q)}$  and  $B_{-(p+q)}$  or segments of the pair  $B_{(p-q)}$  and  $B_{-(p-q)}$ . The  $V_k$ 's are either hexagons or parallelograms. Notice that six of these neighbors are always ordered, from largest imaginary part to smallest imaginary part (top to bottom in the picture), as follows:

$$N_{p+q} \triangleright N_p \triangleright N_q \triangleright z_k \triangleright N_{-q} \triangleright N_{-p} \triangleright N_{-(p+q)}$$

Now, consider the Voronoi partition of  $\mathcal{C}$  given by the half-lattice  $z_1, z_2, z_3, \dots$  and disregard anything below the line  $\mathbb{S}^1 \times \{0\}$ , which we call the  $x$ -axis (see Figures 17 and 20). We emphasize that the point  $z_0 = 0$  is not included. As mentioned earlier, we call the set  $T$  of Voronoi cells that intersect the  $x$ -axis the *first tier*. Cells in  $T$  are therefore not closed, and are not congruent to the cells of the complete planar lattice, which we call *complete*. Any  $V_k \in T$  has two of its boundaries intersecting the  $x$ -axis. We call these two boundaries *walls* of the cell. The maxima of the function  $D$  must occur at intersection points of the walls of cells in  $T$  with the  $x$ -axis. Notice that  $B_{(p+q)}$  cannot be a wall of any  $V_k \in T$  and, since  $N_{-(p+q)}$  is below the  $x$ -axis (otherwise  $V_k$  would be complete),  $B_{-(p+q)}$  cannot be a wall either.

**Lemma 9.1.** *Let  $V_k \in T$ . If  $B_p$  (resp.  $B_{-p}$ ) is a wall of  $V_k$  then  $B_q$  (resp.  $B_{-q}$ ) is the other wall.*

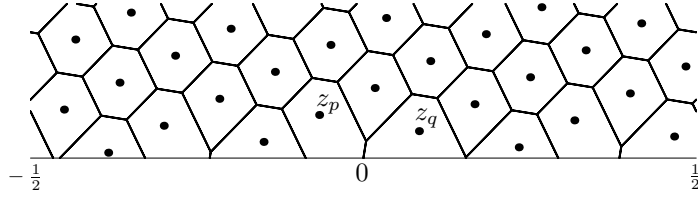


Figure 20: Voronoi partition of a half-lattice  $z_1, z_2, z_3, \dots$ . The cells intersecting the  $x$ -axis form the first tier  $T$ . In this example, from left to right, they are of types  $(q, p)^-$ ,  $(q, p)^+$ ,  $(q, p - q)^-$ ,  $(q, p - q)^+$ , etc. (see definition of these types below).

*Proof.* If  $B_{-p}$  is a wall, then  $N_{-p}$  is above the  $x$ -axis, and therefore so is  $N_{-q}$ . Hence, the other wall is  $B_{-q}$ . If  $B_p$  is a wall, let  $L$  be the bisector of the segment  $\overline{N_p N_{p-q}}$  (see Figure 21). Since  $B_p$  is a wall, the intersection of  $B_p$  and  $L$  must be below the  $x$ -axis. Translating by  $z_{q-p}$ , we have a congruent geometrical situation: the intersection of  $B_q$  and the bisector of  $\overline{N_q N_{-(p-q)}}$  is also below the  $x$ -axis. Therefore  $B_q$  is the other wall.  $\square$

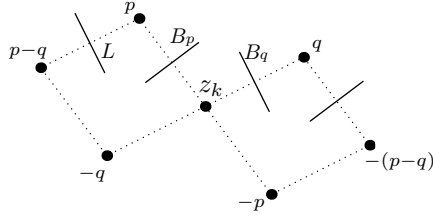


Figure 21: Translating by  $z_{q-p}$ :  $L$  ends up on  $B_q$ .

We now classify the Voronoi cells in  $T$  according to the type of their walls, not taking into account which wall is on the left and which is on the right. Considering the previous lemma, it is easy to check that we can only have the following types:

**Definition.** A cell  $V_k \in T$  is said to be of type

- i)  $(q, p)^-$  if it has walls  $B_{-q}$  and  $B_{-p}$ .
- ii)  $(q, p)^+$  if it has walls  $B_q$  and  $B_p$ .
- iii)  $(q, p - q)^-$  if it has walls  $B_{-q}$  and  $B_{-(p-q)}$ .
- iv)  $(q, p - q)^+$  if it has walls  $B_q$  and  $B_{(p-q)}$ .
- v)  $(q, q)$  if it has walls  $B_q$  and  $B_{-q}$ .
- vi)  $(p - q, p - q)$  if it has walls  $B_{(p-q)}$  and  $B_{-(p-q)}$ .

**Lemma 9.2.** If  $V_k \in T$  and  $k > p$ , then  $V_k$  is of type  $(q, p)^-$ .  $V_p$  is the cell of type  $(q, p - q)^-$  of highest index.

*Proof.* Since  $k > p$ ,  $N_{-q}$  and  $N_{-p}$  are both above the  $x$ -axis. Hence, both  $B_{-q}$  and  $B_{-p}$  are edges of  $V_k$ . They cannot intersect above the  $x$ -axis, otherwise  $V_k \notin T$ . Thus, both are walls and  $V_k$  is of type  $(q, p)^-$ . Finally,  $V_p$  is of type  $(q, p-q)^-$  because  $|z_p| = |z_q|$ , and therefore the bisector of the segment  $\overline{z_p z_q}$  passes through the origin 0. In terms of the neighbors of  $z_p$ , this segment is  $z_p N_{-(p-q)}$  and the bisector is  $B_{-(p-q)}$ . So one of the walls of cell  $V_p$  is  $B_{-(p-q)}$ . Since  $N_{-q}$  is above the  $x$ -axis,  $B_{-q}$  is the other wall, so the cell is of type  $(q, p-q)^-$ .  $\square$

**Lemma 9.3.** *The maximum of  $D$  cannot occur in a cell of type  $(q, p)^-$ .*

*Proof.* Suppose  $V_k$  is of type  $(q, p)^-$ . For every  $V_k \in T$ , let

$$d_k = \max \{D(x) \mid x \in V_k \cap (\mathbb{S}^1 \times \{0\})\}.$$

$d_k$  is the distance between  $z_k$  and one of the intersection points for the walls of  $V_k$  with the  $x$ -axis. Suppose  $d_k$  is given by the intersection point  $Z'$  of the

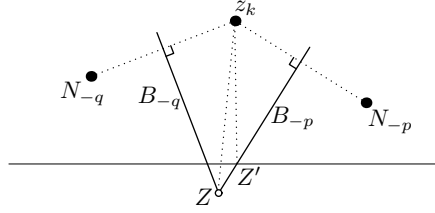


Figure 22: The maximum of  $D$  cannot occur in a cell of type  $(p, q)^-$  since  $|\overline{z_k Z}| < |\overline{z_k N_{-p}}| = |z_p|$ .

wall  $B_{-p}$  and the  $x$ -axis (see Figure 22) (an identical argument applies if it is given by the other wall  $B_{-q}$ ). The intersection point  $Z$  of the bisectors  $B_{-p}$  and  $B_{-q}$  cannot be above the  $x$ -axis because otherwise the cell would not be in  $T$ . We have then two cases: (1)  $Z$  is below the axis, and (2)  $Z$  is on the axis. First suppose that it is below the  $x$ -axis. It is clear in the figure that then  $d_k = |\overline{z_k Z'}| < |\overline{z_k Z}|$ . Since the angle  $Zz_k N_{-p}$  (which is half of angle  $z_p z_0 z_q$ ) is at most  $\frac{\pi}{3}$ , we have  $|\overline{z_k Z}| \leq |\overline{z_k N_{-p}}|$ , and therefore

$$d_k = |\overline{z_k Z'}| < |\overline{z_k Z}| \leq |\overline{z_k N_{-p}}| = |z_p| \leq d_p.$$

So  $d_k$  cannot be the maximum of  $D$ . Suppose now case (2), that  $Z$  is on the axis. So, in Figure 22 we have  $Z = Z'$ . Now, suppose for a moment that our lattice is at a triple point of  $\mathcal{V}$ . We then must have  $V_k = V_p$  because  $V_p$  has its bisectors  $B_{-p}$  and  $B_{-q}$  intersecting on the  $x$ -axis at the lattice point  $z_0 = 0$  and no other cell  $V_k$  for  $k \neq p$  could have a corresponding intersection exactly on the axis. But this is a contradiction because  $V_p$  is not of type  $(q, p)^-$ , so we cannot be at a triple point. If our lattice is not at a triple point of  $\mathcal{V}$ , then angle  $Zz_k N_{-p} < \frac{\pi}{3}$  and therefore we have  $|\overline{z_k Z}| < |\overline{z_k N_{-p}}|$ . Thus  $d_k < d_p$ , and  $d_k$  cannot be a maximum of  $D$ .  $\square$

Notice that if  $V_{k_1}$  and  $V_{k_2}$  are of the same type with  $k_1 < k_2$ , then  $Im(z_{k_1}) < Im(z_{k_2})$  and all the neighbors of  $z_{k_1}$  are below the corresponding neighbors of  $z_{k_2}$ , therefore  $d_{k_1} < d_{k_2}$ . That is, we have proven

**Lemma 9.4.** *If the max value of  $D$  occurs in a cell  $V_k$  of type  $x$ , then  $k$  is the highest index for a cell of same type  $x$ .*

*Proof of Proposition 5.5.* Let  $V_k$  be a cell where the max value of  $D$  occurs in at least one of its walls (In particular,  $k$  is largest index for this type). We know that the type cannot be  $(p, q)^-$ . If the type is  $(q, p - q)^-$  then  $k = p$ . If  $V_k$  is of type  $(q, q)$ , the max must be on the longest wall:  $B_q$ . This wall is  $B_{-q}$  for the neighboring cell. By Lemma 9.3, this neighboring cell could not be  $(q, p)^-$ , so it must be  $(q, p - q)^-$ , and therefore it is  $V_p$ .

If  $V_k$  is of type  $(p - q, p - q)$ , then the max must be on the longest wall:  $B_{p-q}$ . This wall is  $B_{-(p-q)}$  for the neighboring cell, which must then be of type  $(q, p - q)^-$ , and therefore it is  $V_p$ .

If  $V_k$  is of type  $(p, q)^+$ , then the max is not on the wall  $B_p$  because the  $p$ -side neighboring cell is necessarily of type  $(p, q)^-$ . The max is then on wall  $B_q$  of  $V_k$ . For the neighboring cell on this side, this wall must be  $B_{-q}$ . So the type possibilities for this neighboring cell are  $(q, q)$ ,  $(q, p)^-$  or  $(q, p - q)^-$ . It cannot be  $(q, q)$  because the other wall is parallel and higher and it would give a higher value than the maximum. It cannot be  $(q, p)^-$  (by Lemma 9.3), so it must be the third case, and therefore it is  $V_p$ .

Suppose  $V_k$  is of type  $(q, p - q)^+$ . If the max occurs in the  $B_q$  wall, then we reason as in the previous case. Suppose max occurs on the  $B_{p-q}$ -wall. The neighboring cell on this side could either be  $(p - q, p - q)$  or  $(q, p - q)^-$ . It cannot be  $(p - q, p - q)$  because the second wall yields a larger value for  $D$ , so it is of type  $(q, p - q)^-$ , and therefore it is  $V_p$ .  $\square$

## References

- [1] Adler I., A Model of Contact Pressure in Phyllotaxis *J. Theor. Biol.* **45**, (1974), pp. 1-79.
- [2] Adler I., The Role of Mathematics in Phyllotaxis, *Symmetry in Plants* World Scientific, (1998), pp. xiii-xvi.
- [3] Ahlfors L.V., *Complex Analysis*, McGraw-Hill (1966).
- [4] Atela, P., Hotton, S. & Golé, C., Periodicity in Phyllotaxis, *in preparation*.
- [5] Bravais, L. & Bravais, A., *Annales des Sciences Naturelles Botaniques* **7** (1837) pp. 42-110, 193-221, 291-348; **8** (1837), pp. 11-42.
- [6] Douady S., The Selection of Phyllotactic Patterns, *Symmetry in Plants* World Scientific, (1998), pp. 335-358.
- [7] Douady S. & Couder Y., Phyllotaxis as a Self Organizing Iterative Process, Part I, *J. Theor. Biol.* **178**, (1996), pp. 255-274.
- [8] Douady S. & Couder Y., Phyllotaxis as a Self Organizing Iterative Process, Part II, *J. Theor. Biol.* **178**, (1996), pp. 275-294.

- [9] Douady S.& Couder Y., Phyllotaxis as a Self Organizing Iterative Process, Part III, *J. Theor. Biol.* (1996) **178**, pp. 295-312.
- [10] Erickson R. O., The Geometry of Phyllotaxis, *The Growth and Functioning of Leaves*, Cambridge University Press, (1983), pp. 55-88.
- [11] Green P.B., Steele C.R. & Rennich S.C., Phyllotactic Patterns: a Biophysical Mechanism for their Origin, *Ann. Bot.* (1996), pp. 515-27.
- [12] Hardy, G. H. and Wright, E. M., *An Introduction to the Theory of Numbers*, 5th ed. Oxford, England: Clarendon Press.
- [13] Hofmeister W., Allgemeine Morphologie der Gewächse, in *Handbuch der Physiologischen Botanik*, **1** Engelmann, Leipzig (1868), pp. 405-664.
- [14] Hotton, S., *Thesis*, University of California, Santa Cruz (1999).
- [15] Jean R.V., *Phyllotaxis, a Systemic Study in Plant Morphogenesis*, Cambridge University Press (1994).
- [16] Kunz M., *Thèse*, Université de Lausanne, Switzerland (1997).
- [17] Lee, H.W. & Levitov L.S., Universality in Phyllotaxis: A Mechanical Theory, *Symmetry in Plants*, World Scientific, (1998) pp. 619-653.
- [18] Levitov L.S., Energetic Approach to Phyllotaxis, *Europhys. Lett.* **14** (6), (1991), pp. 533-539.
- [19] Longhi E., *Honors Thesis*, Smith College (2000).
- [20] Meicenheimer, R., Relationship Between Shoot Growth and Changing Phyllotaxy of *R. anunculus*, *Amer.J. Bot.* **66** (5), pp. 557-569.
- [21] Meinhardt H., Koch A.J., & Bernasconi G., Models of Pattern Formation Applied to Plant Development, in *Symmetry in Plants* (1998), pp. 723-758.
- [22] Robinson, C., *Dynamical Systems*, CRC Press, (1994).
- [23] Schoute J.C., *Recueil des Travaux Botaniques Néerlandais* **10** (1913), pp. 153-325.
- [24] Schwabe W.W. & Clewer A.G., A Simple Computer Model Based on the Theory of a Polarly Translocated Inhibitor, *J. Theor. Bio.* (1984), pp. 595-619.
- [25] Schwabe W.W., The Role and Importance of Vertical Spacing at the Plant Apex in Determining the Phyllotactic Pattern, *Symmetry in Plants* (1998), pp. 523-535.
- [26] Seneta E., *Non-negative matrices; an introduction to theory and applications*, Wiley (1973).
- [27] Snow M. & Snow R., Minimum Areas and Leaf Determination, *Proc. Roy. Soc.*, **B139**, (1952), pp 545-566.
- [28] Thornley J.H.M., Phyllotaxis I. A Mechanistic Model, *Ann. Bot.*, **39**, (1975), pp 491-507.
- [29] Tucker S.C., Phyllotaxis and Vascular Organization of the Carpels of *Michelia Fuscata*, *Am. J. Bot.* **48** (1961), pp. 60-71.
- [30] Turing A.M., The Chemical Basis of Morphogenesis, *Phil. Trans. Roy. Soc.* **237B** (1952), pp. 37-72.
- [31] Veen A.H. *thesis*, University of Pennsylvania, Philadelphia (1973).

- [32] Young D.A., On the Diffusion Theory of Phyllotaxis, *Journal of Theoretical Biology*, **71** (1978), pp. 421-432.
- [33] Williams R.F., *The Shoot Apex and Leaf Growth*, Cambridge University Press, (1975).
- [34] Zagórska-Marek B., Phyllotaxic Diversity in *Magnolia* Flowers, *Acta Soc. Bot. Poloniae* **63** (1994), pp. 117-137.